

Strength and Ductility Improvement of Recycled Aggregate Concrete by Polyester FRP-PVC Tube Confinement

Chang Gao¹, Liang Huang^{1*}, Libo Yan^{2,3*}, Ruoyu Jin⁴ and Bohumil Kasal^{2,3}

¹College of Civil Engineering, Hunan University, Changsha 410082, China

²Centre for Light and Environmentally-Friendly Structures, Fraunhofer Wilhelm-Klauditz-Institut WKI, Bienroder Weg 54E, Braunschweig 38108, Germany

³Department of Organic and Wood-Based Construction Materials, Technical University of Braunschweig, Hopfengarten 20, 38102 Braunschweig, Germany

⁴School of Environment and Technology, University of Brighton, Cockcroft Building 616, Brighton, UK

*Corresponding authors: Liang Huang. Email: lianghuanghnu@gmail.com and Libo Yan. Email: l.yan@tu-braunschweig.de

Abstract

In literature, studies on recycled aggregate concrete (RAC) with recycled aggregates (RAs) originated from clay brick waste are rare, which is mainly attributed to the much lower compressive strength of the RAC with recycled clay brick aggregates (RAC-RCBA) when comparing with its normal aggregate concrete (NAC) counterpart. Nowadays it is well known that fiber reinforced polymer (FRP) composites as lateral confining materials can improve the strength and ductility of NAC significantly. In this study, FRP confining materials were used to improve the compressive strength and ductility of the RAC-RCBA. Compared with conventional synthetic glass or carbon FRP composites, polyester FRP (PFRP) and Polyvinyl chloride (PVC) are much cheaper and show much larger tensile deformation capacity. Therefore, this study investigated the axial compressive behavior of PFRP and PVC hybrid tube encased RAC-RCBA (i.e., shortened as PFRP-PVC-RAC-RCBA) structure. This PFRP-PVC-RAC-RCBA system consisted of an RAC-RCBA core, encased by a PVC tube directly and the PVC tube was further confined with a PFRP tube (i.e. PFRP tube-PVC-RAC-RCBA specimen) or PFRP strips (i.e. PFRP strip-PVC-RAC-RCBA) at the outermost layer. Uniaxial compression tests were performed on 33 PFRP-PVC-RAC-RCBA and 39 unconfined RAC-RCBA specimens to evaluate and compare the axial compressive behavior of PVC tube encased RAC-RCBA, PFRP tube encased RAC-RCBA, PFRP tube-PVC-RAC-RCBA and PFRP strip-PVC-RAC-RCBA columns. The tested variables included the number of PFRP layers (3-, 6- and 9-layer), the type of PFRP confinement (in the configuration of tube or strips) and the spacing of the PFRP strips (25 and 50 mm). The tested results demonstrated that the PFRP-PVC hybrid confining system enhanced the compressive strength and axial and lateral deformations of the RAC-RCBA pronouncedly, e.g. the increase in strength ranged from 4.5% to 39.6%. The enhancement in strength and deformations was increased with a thicker PFRP tube or strip. Both the PFRP tube-PVC-RAC-RCBA and PFRP strip-PVC-RAC-RCBA showed the similar axial compressive stress-strain behaviors. In addition, the comparison of PFRP tube-PVC-RAC-RCBA with the glass/carbon FRP tube-RAC-RCBA indicated that the GFRP and CFRP tube confinement resulted in much larger enhancement in ultimate compressive strength of RAC-RCBA due to the much larger tensile modulus and strength of these G/CFRP composites. However, PFRP-PVC tube confinement led to much larger axial deformation of the RAC-RCBA compared with the G/CFRP tube confinement due to the much larger tensile strain of the PFRP and PVC material. Furthermore, design-oriented compressive stress-strain models were developed for PFRP-PVC-RAC-RCBA specimens.

Keywords: Recycled aggregate concrete (RAC); Recycled clay brick aggregates (RCBA); Polyester fiber reinforced polymer (PFRP); PVC; Dual confinement; Compressive behavior

52 **Nomenclature**

<i>RAC</i>	Recycled aggregate concrete	d	Diameter of cylindrical core concrete
<i>RCBA</i>	Recycled clay brick aggregate	f_{co}	Peak stress of unconfined RAC-RCBA
<i>RAs</i>	Recycled aggregates	ϵ_{co}	Axial strain of unconfined RAC-RCBA at peak stress
<i>NAC</i>	Natural aggregate concrete	f_{ct}	Peak stress of confined specimens
<i>NAs</i>	Natural aggregates	ϵ_{ct}	Lateral strain of confined specimens at peak stress
<i>FRP</i>	Fiber reinforced polymer	ϵ_l	Axial strain of confined specimens at peak stress
<i>PFRP</i>	Polyester FRP	f_l	Lateral confining pressure of FRP
<i>GFRP</i>	Glass FRP	f_{cu}	Ultimate stress of the confined specimens
<i>CFRP</i>	Carbon FRP	ϵ_{cu}	Ultimate axial strain of the confined specimens at ultimate stress
<i>AFRP</i>	Aramid FRP	μ	Ductility indices
<i>BFRP</i>	Basalt FRP	μ_t	Dilation rate
<i>PVC</i>	Poly Vinyl chloride	f_l'	Lateral confining pressure of the composite confinement on concrete core
<i>RC</i>	Reinforced concrete	f_{lf}	Effective lateral confining pressure provided by PFRP
<i>AVG</i>	Average value	f_{lp}	Lateral confining pressure provided by PVC
<i>COV</i>	Coefficients of variation	E_{pvc}	Elastic modulus of the PVC tube
<i>SD</i>	Standard deviation	ϵ_{pvc}	Tensile strain in the hoop direction of the PVC tube
D_1	Diameter of core RAC	t_{pvc}	Thickness of the PVC tube
D_2	Diameter of PVC tube	n	Number of PFRP strips
H	Height of concrete cylinders	k_e	Effective confining coefficient of the PFRP strip
E_{frp}	Elastic modulus of PFRP tube	Ae	Effective confining area of the core concrete
ϵ_{frp}	Tensile strain in the hoop direction of PFRP tube	A	Gross area of specimens including the core concrete and external hybrid tube
t_{frp}	Thickness of PFRP tube	m	Number of zone without confinement among PFRP strip
t_{frp}'	Equivalent PFRP thickness for PFRP strip-PVC-RAC-RCBA cylinders	s	Spacing distance of the PFRP strip
b_{frp}	Width of PFRP strip	λ	Related eigenvalue of ultimate stress and the elastic modulus of confined materials and core concrete
f_l	Lateral confining pressure	E_c	Elastic modulus of the RAC-RCBA
f_{frp}	Tensile strength of FRP	E_l	Effective lateral confining stiffness of the hybrid PFRP-PVC tube
t_{frp}	Thickness of FRP		

53

54 **1 Introduction**

55 The process of urbanization generated a large amount of construction and demolition waste
 56 (CDW) which caused environmental pollution issues and difficulties to dispose those waste.

57 An abundant utilization of recycled aggregate concrete (RAC) could not only solve the
58 disposal issue of CDW but also reduce the consumption of natural resources [1-2]. RAC is an
59 environmentally friendly concrete in which part or all the natural aggregates (NAs) are
60 replaced by recycled aggregates (RAs) [2]. RAs are mostly sorted from crushed CDW. In
61 literature, most research of RAC focused on the use of RAs originating from old concrete
62 blocks. Indeed, except for the old concrete waste, clay brick waste also accounted for a large
63 portion of the CDW, i.e. up to 30-40% [3-4]. So, if recycled clay brick aggregates (RCBA)
64 originated from clay brick wastes can be used to produce RAC as structural concrete, this will
65 be a significant step for the development of sustainable concrete industry. However, RCBA
66 typically exhibited weaknesses when being used to produce RAC, i.e., high porosity and
67 variation in quality [5-9]. For example, because of the high porosity of RCBA, the crushing
68 index and water absorption of RAs can be significantly larger than those of NAs, i.e. the
69 crushing index and water absorption of RCBA might be 60% and 700% larger than those of
70 NAs, respectively. This can cause poor mechanical properties of the resulting RAC such as
71 the reduction in load carrying capacity and stiffness and increase in creep and shrinkage of the
72 RAC [5-7]. In addition, the complexity of RCBA's source results in the dispersion and
73 uncertainty of the mechanical properties of RAC in the aspects of flow ability, strength and
74 durability [8]. Thus, the mechanical properties of RAC-RCBA should be improved to expand
75 the range of their application considering the social and environmental benefits to use RCBA
76 [9].

77 It has been widely accepted that confined concrete is an effective way to improve mechanical
78 properties of concrete [10-14]. Fiber reinforced polymer (FRP) composites such as glass FRP
79 (GFRP), carbon FRP (CFRP), and other FRP composites, i.e., basalt FRP (BFRP) [71] and
80 steel fibers [72], as one of the most effective confining materials for concrete, have been
81 widely used to improve the strength and ductility of natural aggregate concrete (NAC).
82 Concrete filled FRP tube (CFFT) is a hybrid structure that the pre-fabricated FRP tubes serve
83 as permanent formworks of fresh NAC and offer lateral confining pressure to enhance the
84 strength and ductility of the NAC core [13-19]. In literature, some recent studies have
85 investigated the behavior of RAC filled FRP tube [20-24]. For example, Gao et al. [21]
86 compared the compressive behavior of CFRP tube and GFRP tube encased RAC cylinders.
87 Ozbakkaloglu et al. [22] concluded that the RAC filled FRP tube with circular cross-sections
88 showed higher compressive strength when compared with the specimens with square cross-
89 sections. Chen et al. [23] stated that the replacement ratio of RAs had a limited effect on the
90 CFRP confinement effectiveness for RAC. Choudhury et al. [24] concluded that the initial
91 stiffness of plain RAC-RCBA columns increased significantly with GFRP jacket confinement.
92 Ardavan et al. [25] even found that CFRP strengthening increased the load capacity of the
93 RAC beams and can be designed more load-affordable than the NAC beams.

94 However, synthetic GFRP and CFRP are expensive in their initial material price, non-
95 degradable and non-recyclable. Against this background, recent researchers have used new
96 confining materials to gain environmental and economic benefits. Polyester fiber, as one
97 textile fiber, has advantages of large production, low price, degradability and appropriate
98 mechanical properties [26-31]. Therefore, polyester FRP (PFRP) has been used to confine
99 concrete columns. For example, Dai et al. [32] investigated the axial compressive behavior of
100 PFRP tube encased NAC and was compared with aramid FRP (AFRP) tube confined NAC.
101 This study showed that the PFRP confinement might not enhance the strength of the concrete
102 as much as that of the AFRP but PFRP improved the ultimate strain of the NAC more
103 pronouncedly and exhibited superior in cost performance. Ispir [33] stated that the PFRP
104 confinement improved the strength and ultimate axial strain of confined NAC and had high
105 deformation capacity which could be a good alternative in repairing or strengthening for
106 seismic-resistant RC structures. Saleem et al. [34-35] concluded that PFRP encased NAC
107 columns exhibited highly ductile behavior owing to the large rupture strain of the PFRP.
108 Pimanmas et al. [36] demonstrated that the stress-strain behavior of PFRP tube encased NAC
109 presented apparent softening stage and the compressive strength increased with more PFRP

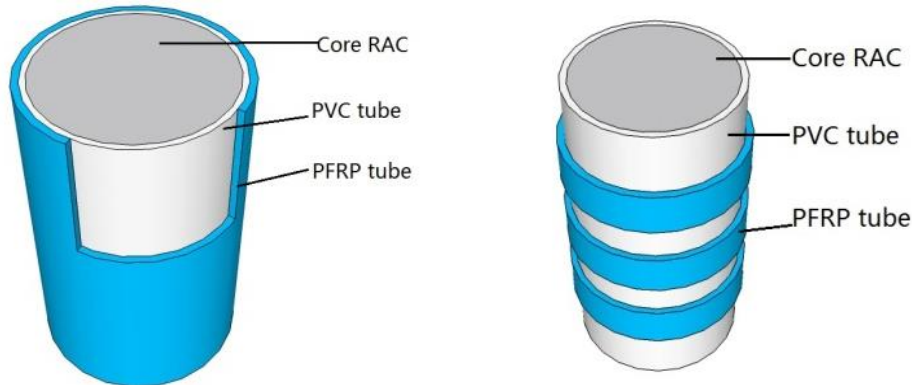
110 thickness. Huang et al. [37] investigated the effect of PFRP confinement ratios and concrete
111 strength on compressive behavior of PFRP encased NAC. Huang et al. [38] also investigated
112 the effects of slenderness and size of on the PFRP tube confined concrete cylinders.

113 Poly Vinyl chloride (PVC) materials were also extensively utilized in the construction
114 industry as concrete moulds or pipes due to the high production, low price and stable service
115 performance [39-41]. The apparent merits of PVC materials include: (1) excellent corrosion
116 resistant, durability and mechanical stability, (2) smooth surface and good consistency with
117 other materials, e.g., concrete, water and acids, (3) large ultimate strain (i.e., ductile), (4) high
118 electrical insulation, (5) low diffusion for humidity, (6) low creep deformation, and (7) easy
119 for machining, cutting, gluing for fabrication versatility. Research [42] showed that PVC tube
120 did not lose strength significantly under the thermocycling tests. Nowack et al. [43] conducted
121 tests on PVC tubes that were buried under soil for 60 years. They found that the PVC tubes
122 did not deteriorate and was expected to serve for a further 50 years. Ranney et al. [44] found
123 that PVC tubes could adequately resist the influence of chloridion, salts, freeze thawing and
124 other chemical effects and maintain their long-term durability. Kurt [45] proposed PVC tube
125 encased NAC for structural application and concluded that the PVC confined NAC performed
126 like spiral steel confined concrete to afford effective ductility enhancement. Toutanji et al.
127 [46-48] conducted experiments on mechanical properties and durability of GFRP-PVC tube
128 encased NAC and found that the hybrid confinement enhanced the load carrying capacity and
129 ductility of concrete and provided excellent durability even under high corrosive conditions.
130 Wang et al. [49] stated that the thermal conductivity of PVC was only 0.45-0.6% of steel
131 which would afford more stable condition without apparent change of temperature for
132 concrete curing. Gupta et al. [50] investigated the PVC tube encased NAC under sea water for
133 six months. The tested results indicated that no degradation in the strength and ductility of the
134 confined NAC was observed and the PVC tube served as a safe jacket to protect the core
135 concrete. Gathimba et al. [51] demonstrated that the confinement effectiveness of PVC
136 confined NAC is dependent on the strength of concrete where the confinement ratio reduced
137 with a higher strength of the concrete. Jiang et al. [52] explored the influence of slenderness
138 ratio on CFRP-PVC tube encased NAC under uniaxial compression.

139
140 Based on the discussions above, it can be concluded that the cost-effective PFRP-PVC hybrid
141 tube confinement has the potential to improve the mechanical properties of RAC-RCBA.
142 Thus, in this study, PFRP-PVC tube encased RAC-RCBA (termed as PFRP-PVC-RAC-
143 RCBA), for the first time, was proposed to improve the mechanical properties of RAC-RCBA.
144 This PFRP-PVC-RAC-RCBA system was consisted of a PFRP (at the outer layer of the tube)
145 and PVC (at the inner layer of the tube) hybrid tube and an RAC-RCBA infill as illustrated in
146 Fig.1 (a). In this system, the inner PVC tube not only serves as the permanent formwork for
147 the fresh RAC-RCBA but also serves as the permanent formwork for fabricating the outer
148 PFRP tube using the typical hand lay-up process [59]. It should be pointed out here that for
149 the typical hand lay-up process to make FRP tube, a mould (such as made of PVC or
150 aluminum tube) is needed and then the resin-impregnated fiber fabrics are wrapped onto the
151 mould. When the FRP tube is fully consolidated, it will be demoulded from the PVC or the
152 aluminum tube. In the case of PFRP-PVC hybrid tube situation, the demoulding process of
153 PFRP tube from the initial mould (e.g. a PVC tube) is not needed and in turn the construction
154 time can be further reduced. Specifically, the objectives of this study included:

- 155 1) To obtain the optimal design mix ratio for RAC-RCBA cylinder by testing different
156 replacement ratios of the RCBAs and different water-cement ratios;
- 157 2) To investigate the material properties of the PFRP and PVC composites with different
158 thicknesses by flat coupon tensile tests;
- 159 3) To investigate the axial compressive behavior of PFRP-PVC-RAC-RCBA cylinders
160 considering different column parameter effects: the number of PFRP layers (3, 6 and 9-
161 layer), type of the PFRP confinement (i.e. in the configuration of PFRP tubes (see Fig1(b))

162 and strips (see Fig 1(b)) and the spacing distance of the PFRP strips (25 mm and 55 mm);
 163 and
 164 4) To develop stress-strain modes for PFRP-PVC-RAC-RCBA in axial compression by the
 165 regression analysis and iterative computations of the tested results.
 166



a) PFRP tube-PVC-RAC-RCBA cylinder b) PFRP strip-PVC-RAC-RCBA cylinder
 Fig 1 PFRP-PVC-RAC-RCBA schematic diagram

167

168 **2 Experimental works**

169 **2.1 Material properties of RAC-RCBA**

170 *2.1.1 RAs*

171 The RAs used in the experiments are shown in Fig.2, which were a mixture of RAs from
 172 RCBAAs and from recycled old concrete waste. The portion of the RCBAAs accounted for 55%
 173 of the RAs by mass. The properties of the RAs are listed in Table 1. The crushing index of the
 174 RAs was 17.3% which meets the demands of crushing indexes of RAs specified in the
 175 Chinese National Standard GB/T 25177-2010 [53]. The crushing index of the natural
 176 aggregates was 10.7%.

177

178

Table 1 Physical property of RAs

Partial size (mm)	Density (kg/m ³)	Porosity (%)	Water absorption (%)	Moisture content (%)	Crushing index (%)
5~10	1140	10	14.8	6.5	17.3



Fig.2 RAs used

179 *2.1.2 Compression tests of RAC-RCBA*

180 To evaluate the effects of replacement ratios of RAs and water-cement ratios on the
 181 compressive strength of RAC-RCBA, two groups of experimental works were conducted:
 182 Group A and Group B. The Group A consisted of three categories of RAC-RCBA cubes
 183 ($150 \times 150 \times 150 \text{ mm}^3$) corresponding to three different replacement ratios of RCBA (i.e., 50%,
 184 70% and 100%). For each category of the specimens, six RAC-RCBA cubic specimens were
 185 constructed for the axial compression test. The details of the mix proportions of Group A are
 186 listed in Table 2. The Group B consisted of three categories of RAC-RCBA cubes
 187 ($150 \times 150 \times 150 \text{ mm}^3$) corresponding to three different water-cement ratios (i.e., 0.46, 0.50
 188 and 0.56). For each category, six RAC-RCBA cubic specimens were also constructed for the
 189 axial compressive test. The details of the mix proportions of Group B are listed in Table 3. In
 190 Tables 2 and 3, r indicates the replacement ratio of the RAs for the natural aggregates and
 191 ω/c indicates the water-cement ratio. In this study, vibratory mixing technology was applied
 192 to produce the RAC-RCBA by using a DT60 double-horizontal shafts mixer. The RAC-
 193 RCBA with vibratory mixing technology showed better in fluidity, load carrying capacity and
 194 durability [56-57]. The vibratory mixing technology combined the vibratory function into the
 195 traditional concrete stir to accelerate the stirring velocity, promoted the uniform distribution
 196 of the aggregates and accelerated the hydration process of the cement to enhance the bond
 197 between cement and aggregates. The crafts of vibratory mixing technology referred to a
 198 secondary stirring: the whole cement, aggregates and half of the water were poured into the
 199 mixer and rotated adequately for about 8-10s in the first step of stirring, then the left half of
 200 the water was poured in and mixed for 30s for the second step of stirring. The fully mixed
 201 RAC-RCBA was poured into the moulds and compacted by vibrator. After pouring, all
 202 specimens were covered by soaking wet cloth and watered three times per day for 28 days.

203
 204 Table 2 RAC-RCBA mix proportion of group A

No.	ω/c	Water (kg/m^3)	Cement (kg/m^3)	Fine aggregate (kg/m^3)	Coarse aggregate (kg/m^3)	RCBA (kg/m^3)	r
1	0.40	237.5	600.9	520.2	0	1041.4	100%
2	0.40	237.5	600.9	520.2	312.4	729.0	70%
3	0.40	237.5	600.9	520.2	520.7	520.7	50%

205
 206 Table 3 RAC-RCBA mix proportion of group B

No.	ω/c	Water (kg/m^3)	Cement (kg/m^3)	Fine aggregate (kg/m^3)	Coarse aggregate (kg/m^3)	RCBA (kg/m^3)	r
1	0.46	292.3	635.4	571.0	310.1	731.0	70%
2	0.50	315.4	626.0	545.5	300.8	701.8	70%
3	0.56	362.1	650.0	545.5	301.0	702.1	70%

207
 208
 209 The cubic specimens at 7-day were tested under a DYE-2000 electro hydraulic compression
 210 machine to determine the compressive strength. The tested results of the RAC-RCBA cubes
 211 in Group A are illustrated in Fig. 3 and the coefficients of variation (COV) of the tested
 212 compressive strength obtained from six cubic specimens are also presented to demonstrate the
 213 degree of dispersion of tested results, which were calculated as the ratio of the standard
 214 deviation and the mean value of the strengths. It shows that the compressive strength of the
 215 RAC-RCBA with 70% replacement ratio of RAs was the largest. The tested strengths of the
 216 RAC-RCBA specimens in the Group B are listed in Fig.4. It shows that for RAC with RAs
 217 replacement ratio of 70%, the compressive strength showed a descending tendency with an
 218 increase of the water-cement ratios from 0.40 to 0.50. The further increase of the water-
 219 cement ratio from 0.50 to 0.56 resulted in a slight increase in the strength of the RAC. The
 220 slight increase in the strength for specimen with water/cement ratio of 0.56 might be
 221 attributed to the following two-folds: (1) the high porosity and water absorption of the RCBA
 222 limited the rates of hydration reaction of cement. With an increase of the water/cement ratio,
 223 the RCBA was saturated with water which weakened the hydration reaction of the cement and

224 in turn increased the compressive strength slightly, (2) the old brick powder and old mortar
 225 adhered at surface of the RCBA had a negative effect on the hydration reaction of the cement.
 226 For specimen with a larger water/cement ratio of 0.56, the old powder and old mortar limited
 227 the rates of hydration of the cement which resulted in a slight increase of the compressive
 228 strength. In addition, the RAC-RCBA with water-cement ratio of 0.40 and RAs replacement
 229 ratio of 70% had the highest compressive strength among all the categories in Group A and
 230 Group B.
 231

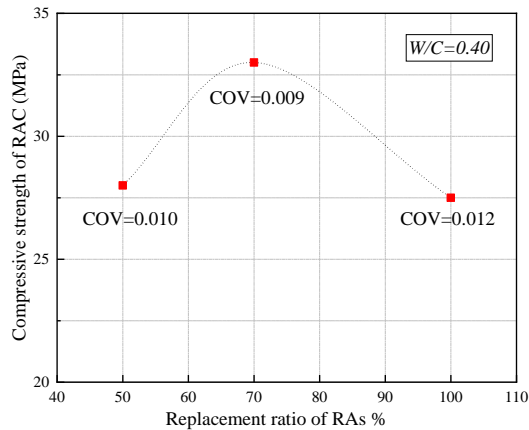


Fig.3 The influence of r on compressive strength of RAC-RCBA

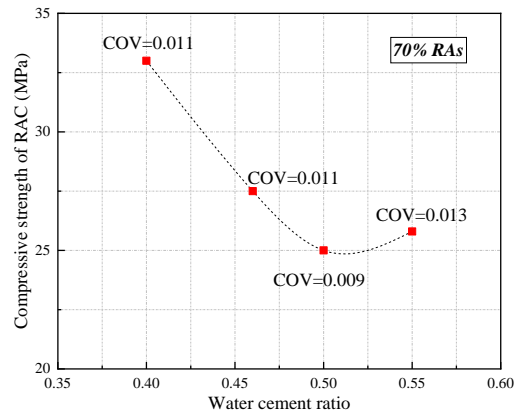


Fig.4 The influence of w/c on compressive strength of RAC-RCBA

232
 233 The failure modes of RAC-RCBA cubes are shown in Fig.5. In general, the experimental
 234 observations indicated that all the RAC-RCBA specimens in Group A and Group B presented
 235 a diagonal pyramid rupture face as illustrated in Fig 5(b), which was like that of the NAC
 236 counterpart. Compared with the NAC, most of the RCBA in the RAC were crushed and
 237 broke under the compressive load, while most of the coarse NAs still maintained intact. This
 238 phenomenon can be interpreted by the much lower crushing index of NAs compared with that
 239 of the RAs.
 240



a) Failure pattern of RAC-RCBA cube b) Rupture face of RAC-RCBA cube
 Fig.5 Failure mode of RAC-RCBA cube

241
 242

243 2.2 Preparation of PFRP-PVC-RAC-RCBA

244 2.2.1 Test matrix

245 To investigate the axial compressive behavior of PFRP-PVC-RAC-RCBA, 36 cylindrical
 246 specimens (i.e. 3 unconfined RAC-RCBA and 33 confined RAC-RCBA cylinders) were
 247 constructed and tested under axial compression. The tested variables included the number of
 248 PFRP layer (i.e. 3, 6, and 9-layer), the type of the PFRP confinement (i.e. in the
 249 configurations of tube (Fig. 1(a) and strips (Fig. 1(b))) and the spacing distance of the PFRP

250 strips (i.e. 25 mm and 50 mm). These specimens were classified into one category of
 251 unconfined RAC-RCBA, one category of PVC tube encased RAC-RCBA (i.e. PVC-RAC-
 252 RCBA), one category of PFRP tube encased RAC-RCBA (i.e. PFRP-RAC-RCBA), and nine
 253 categories of PFRP-PVC-RAC-RCBA (i.e. 3P-T, 3P-S25, 3P-S50, 6P-T, 6P-S25, 6P-S50, 9P-
 254 T, 9P-S25, and 9P-S50). For each category three identical specimen were tested. The details
 255 of all the specimens are listed in Table 4. For the PFRP tube-PVC-RAC-RCBA specimens,
 256 the letter P with a figure in the front was used to represent the specimens, i.e. 3P-T, 6P-T and
 257 9P-T indicates 3-layer, 6-layer and 9-layer PFRP tube-PVC-RAC-RCBA specimens,
 258 respectively. For PFRP strip-PVC-RAC-RCBA specimens, the figure in front of the letter P
 259 denotes the number of layers of the PFRP strip and the figure behind the letter S denotes the
 260 spacing distances of the PFRP strip, e.g., the specimen code 3P-S25 denotes PFRP strip-PVC-
 261 RAC-RCBA specimen with 3 layers of PFRP strips and spacing distance of 25 mm. The
 262 diameter of the core RAC D_1 and the height of core RAC are 152 mm and 305 mm,
 263 respectively. The external diameter of the PVC tube D_2 and the thickness of PVC tube is 160
 264 mm and 4 mm, respectively.

Table 4 Characteristics of tested cylindrical specimens

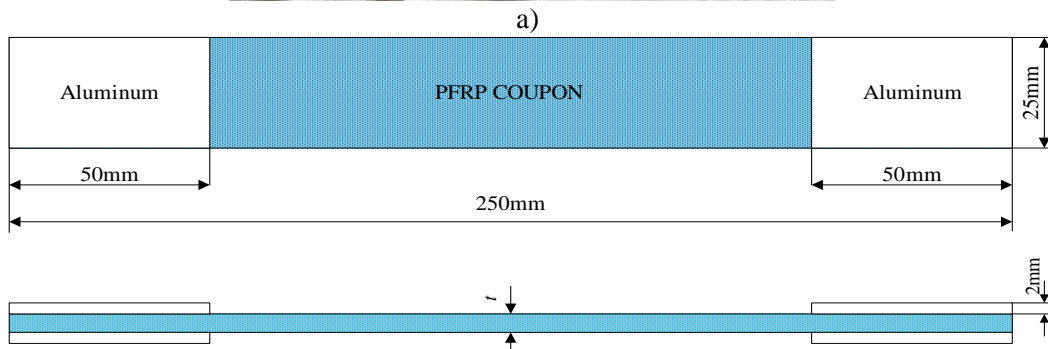
No.	Specimen	D_1 of core RAC (mm)	D_2 of PVC tube (mm)	Height (mm)	PFRP layer	PFRP confined modes
1	RAC-RCBA	152	—	305	—	—
2	PVC-RAC-RCBA	152	160	305	—	—
3	PFRP-RAC-RCBA	152	—	305	6	Tube
4	3P-T	152	160	305	3	Tube
5	3P-S25	152	160	305	3	spacing distance 25mm
6	3P-S50	152	160	305	3	spacing distance 50mm
7	6P-T	152	160	305	6	Tube
8	6P-S25	152	160	305	6	spacing distance 25mm
9	6P-S50	152	160	305	6	spacing distance 50mm
10	9PT	152	160	305	9	Tube
11	9P-S25	152	160	305	9	spacing distance 25mm
12	9P-S50	152	160	305	9	spacing distance 50mm

267
 268 For all the confined RAC-RCBA, the concrete mix proportion of the RAC-RCBA followed
 269 the specimen with the highest compressive strength given in Section 2.1, namely, the RA
 270 replacement ratio of 70% and the water-cement ratio of 0.40. The tested compressive strength
 271 of the RAC-RCBA at 28-day based on six identical specimens was 30.6 MPa, and the
 272 standard deviation was 0.45 MPa.

274 2.2.2 PFRP materials

275 The bidirectional polyester textile with an areal density of 250 g/m² and a thickness of 0.55
 276 mm were used to fabricate the PFRP tubes. Fig.6 (a) shows the polyester textile used for the
 277 study. The textile was made by continuous polyester fibre filaments and these long fibres
 278 were oriented in the wrap and weft directions of the textile with an angle of 90°. According to
 279 ASTM D3039-M08 [54], flat coupon tensile tests were conducted on PFRP laminate to obtain
 280 the tensile strength, strain and modulus. The details of the PFRP laminates used for the flat-
 281 coupon tests are shown in Fig. 6. Aluminum bars of 50 mm in length and 25 mm in width
 282 were glued to the both ends of the PFRP laminates to avoid premature failure. The PFRP

283 laminates with 1, 3, 6 and 9 layers of polyester fabric were tested under the tensile load by
 284 using the MTS CMT4204 universal testing machine.
 285



b) Dimension of the PFRP flat coupon

Fig 6 (a) The bidirectional polyester textile and (b) Dimension of the PFRP flat coupon

286
 287
 288
 289
 290
 291
 292
 293

2.2.3 PVC materials

The 4 mm-thick PVC tubes were used for the PVC-RAC-RCBA, PFRP tube-PVC-RAC-RCBA and PFRP strip-PVC-RAC-RCBA specimens. Tensile tests were also carried out on the PVC flat coupon to determine their tensile properties. The size of the PVC coupon used for the tensile test is shown in Fig.7 according to the GB/T 8804.2-2003 [55], where $A=115\text{mm}$, $B=25\text{mm}$, $C=33\text{mm}$, $D=6\text{mm}$, $E=14\text{mm}$, $F=25\text{mm}$, $G=25\text{mm}$, $H=80\text{mm}$ and $I=4\text{mm}$, respectively.

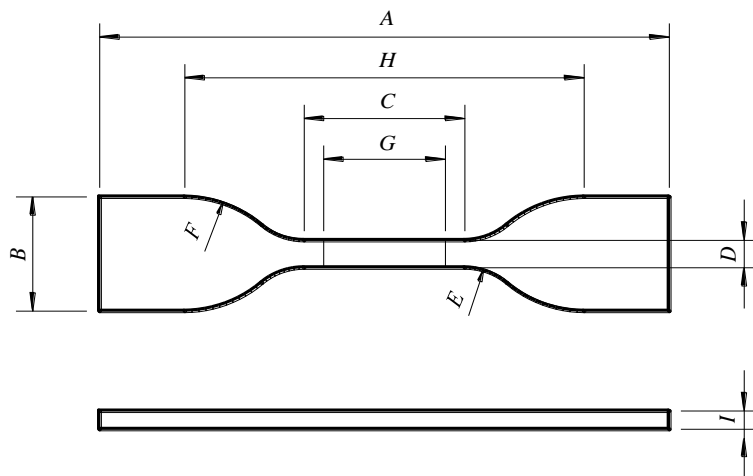


Fig. 7 The dimension of the tested PVC coupon

294
 295

2.2.4 Tensile behavior of PFRP, PVC and comparison with synthetic C/GFRP

296 In this study, the tensile properties of PFRP and PVC were compared with the synthetic
 297 GFRP and CFRP composites which used for GFRP and CFRP tube confined RAC-RCBA
 298 [21]. The tensile stress-strain curves of PFRP, PVC and GFRP and CFRP obtained from flat-
 299 coupon tensile tests are shown in Fig. 8, 9 and 10. The PFRP composites showed a nonlinear
 300 response until the peak stress and then the specimens failed suddenly, which was independent
 301 of the thickness of the PFRP laminate. The PVC showed an initial linear response to the level
 302 of the peak stress and followed by a stress plateau with significant enhancement in the tensile
 303 strain, indicating a ductile behavior. For both the GFRP and CFRP composites, their curves
 304 exhibited an approximate elastic response until the peak stress. For both the GFRP and CFRP
 305 composites, their tensile stress-strain curves exhibited an approximate elastic response until
 306 the peak stress. The damage of the CFRP and GFRP composites in tension was a progressive
 307 and brittle failure process. More details on the progressive degradation failure process of FRP
 308 composites and how to model the progress numerically were introduced by Riccio et al. [68-
 309 70]. The tensile properties of PFRP, PVC, GFRP and CFRP composites are listed in Table 5.
 310 The tensile strength, ultimate strain and elastic modulus were the mean value of the tested
 311 results from the flat-coupon tensile tests and the standard deviations are given to present the
 312 dispersion of the tested results. The tensile modulus and tensile strength of GFRP and CFRP
 313 were significantly larger than those of PFRP and the PVC. However, the tensile strain at
 314 break of PVC and PFRP were much larger than those of the CFRP and GFRP, e.g. the tensile
 315 strain of PVC was 10 times that of the GFRP. In addition, an increase in the thickness of the
 316 PFRP composite resulted in an increase in tensile strength and modulus, but a slight reduction
 317 in the tensile strain. The polymer resin used for PFRP, CFRP and GFRP were the same, i.e.
 318 epoxy matrix with a commercial name of JN-C3P adhesive obtained from GOODBOND
 319 construction technic co., Ltd in China. The tensile strength, compressive strength, flexural
 320 strength and tensile elastic modulus of the JN-C3P resin provided by the supplier are 55 MPa,
 321 83.6 MPa, 75 MPa and 3.5 GPa, respectively.
 322

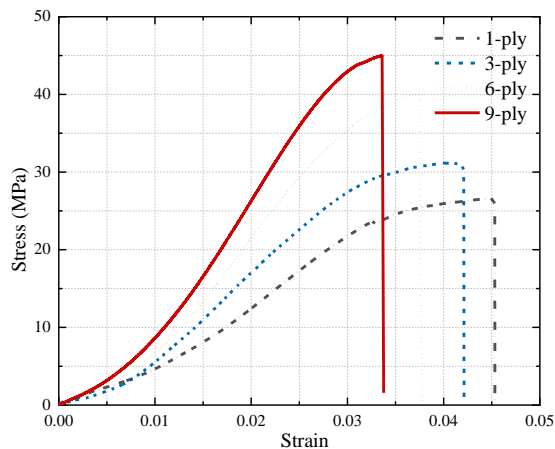


Fig 8 Tensile stress-strain behavior of PFRP

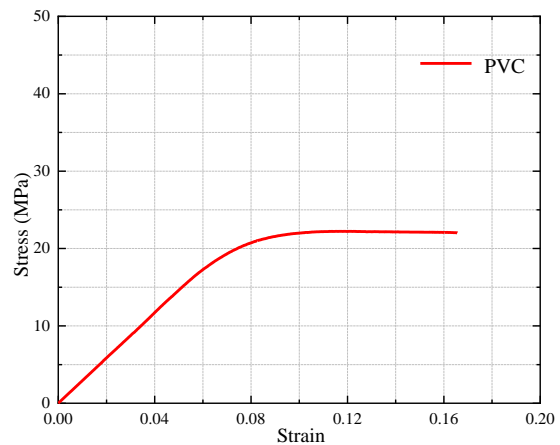


Fig. 9 Tensile stress-strain behavior of PVC

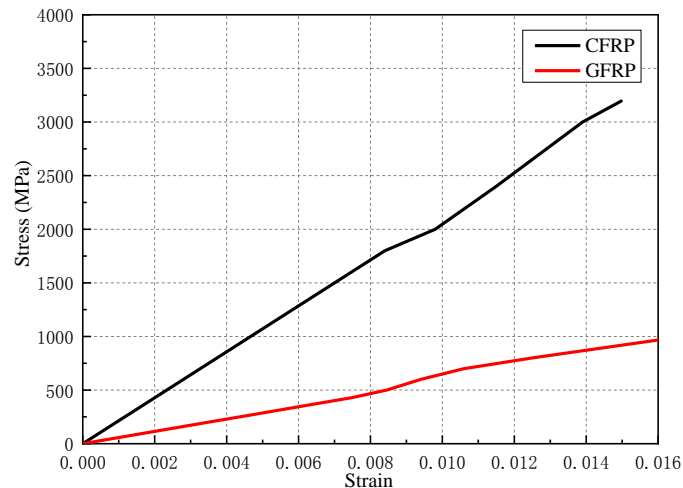


Fig. 10 Tensile stress-strain behavior of CFRP and GFRP [21]

323
324

Table 5 Tensile properties and standard deviation (SD) of PFRP, PVC, GFRP and CFRP composites

Group	Thickness of FRP (mm)	Tensile strength (MPa)	SD (MPa)	Ultimate strain (%)	SD (MPa)	Elastic Modulus (GPa)	SD (MPa)
PFRP1	0.66	27.1	1.5	4.4	0.4	0.9	0.08
PFRP3	1.72	31.1	1.3	4.1	0.2	1.2	0.10
PFRP6	3.18	41.7	1.7	3.8	0.1	1.6	0.12
PFRP9	5.12	45.1	1.4	3.4	0.2	2.0	0.13
PVC	4.00	22.5	0.7	16.0	0.1	0.3	0.03
GFRP	2.62	967.0	-	1.6	-	60.8	-
CFRP	0.96	3200.0	-	1.5	-	213.0	-

325
326

2.3 Fabrication of confined specimens

327 The PVC tube and the polyester fabrics were firstly cut into designated size based on the
328 dimension of the specimens listed in Table 4. The PFRP tubes and PFRP-PVC tubes were
329 produced by a hand lay-up process as illustrated in Fig. 11[38]. The fabrication of the PFRP
330 tube by hand lay-up process mainly included the following steps: 1). Cut polyester textile to
331 designated size based on the diameter of the polymer FRP tube used, 2) surface preparation of
332 hollow PVC tube mould with a thin release plastic film for easy demould, 3) preparation of
333 epoxy mixture, 4) wrapped epoxy-impregnated polyester fabric to the PVC mould, 4) curing
334 of the PFRP tubes, and 5) demoulding PFRP tube from the PVC mould. For the PFRP-PVC
335 tube with PFRP tube or PFRP strips, the process was similar. The PVC tube was used as the
336 mould directly and then the epoxy-impregnated polyester fabrics were wrapped into the PVC
337 tube to make the PFRP-PVC tube. For the fabrication of PFRP strip-PVC tube, the position of
338 polyester fabric strip was initially oriented and labelled on the PVC tube. The air bubble and
339 additional epoxy resin were squeezed out when the PFRP sheets were rolled onto the PVC
340 tube. For all the confined RAC-RCBA specimens, vibratory mixing technology was used as
341 described in Section 2.1.2. To avoid the premature failure of the confined specimens, two
342 narrow PFRP strips were wrapped on both ends of the PFRP-RAC-RCBA, PVC-RAC-RCBA
343 and the PFRP -PVC-RAC-RCBA specimens.



a) PFRP strip-PVC tube

b) PFRP tube

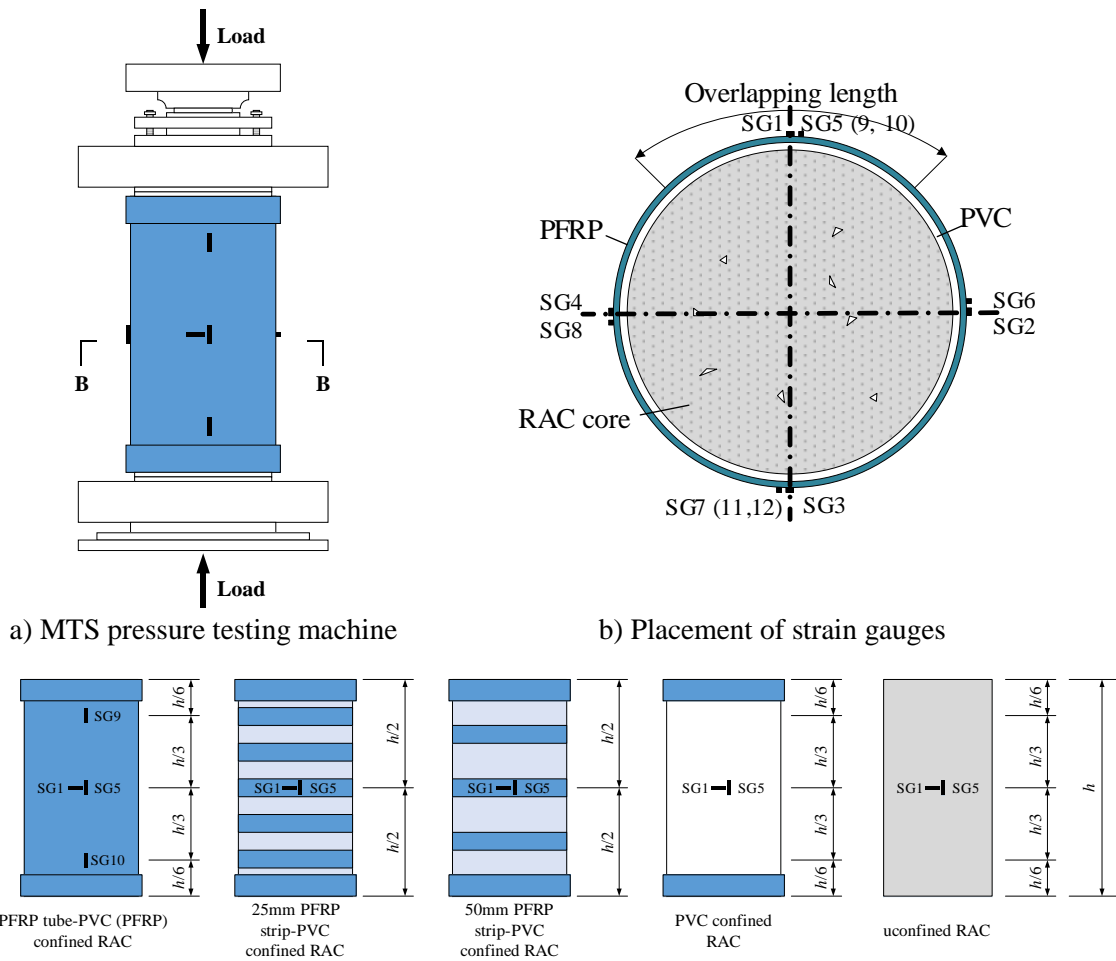
c) All the confined specimens

Fig.11 Fabrication of the specimens

344
 345
 346
 347
 348
 349
 350
 351
 352
 353
 354
 355
 356

2.4 Test instrumentation and procedures

The MTS SANS YAW6506 electro-hydraulic testing machine was used for the uni-axial compression tests (Fig. 12(a)). The loading process was executed by a displacement-control. As illustrated in Fig. 12(b)-(c), four axial strain gauges (i.e., SG1, SG2, SG3, SG4) and four lateral strain gauges (i.e., SG5, SG6, SG7, SG8) were installed on the mid-height of the cylinders for measurement of axial strain and hoop strain, and two extra axial strain gauges were installed on each end of PFRP tube-PVC-RAC-RCBA cylinders (i.e., SG9 and SG11 at the top of PFRP tube-PVC-RAC-RCBA specimens, SG10 and SG12 at the bottom of PFRP tube-PVC-RAC-RCBA specimens), respectively. The applied load and vertical deformation were recorded by MTS system of the compression testing machine. The axial strain, lateral strain, applied load and vertical deformation were measured and recorded simultaneously.



c) Elevation of strain gauges on specimens
 Fig.12 Test instrumentation

357
 358
 359
 360
 361
 362
 363
 364
 365

3 Results and discussion

3.1 Failure modes

For the unconfined RAC-RCBA cylinders, the cracks emerged around the surface of the cylinders after the applied load was up to 40% of its peak strength. The load decreased rapidly after reached its peak strength f_{co} and the cylinders finally failed in a brittle manner with several major vertical cracks (as illustrated in Fig 13(a)). For PVC-RAC-RCBA (i.e. only with PVC tube confinement) specimens, the specimens failed with several longitudinal cracks at the PVC tube and the tube were bulged apparently as illustrated in Fig. 13(b). The obvious bulge of the PVC tube might be caused by the significant lateral expansion of the inner RAC-

366 RCBA core due to the confinement provided by the PVC tube, which possessed a
 367 significantly large tensile strain (Table 5). For the PFRP-RAC-RCBA, only a single
 368 longitudinal crack appeared along the PFRP tube, no obvious bulging of the tube was
 369 observed, as shown in Fig.13(c). This phenomenon in the different level of bulge of the PFRP
 370 and PVC tube might be interpreted by the less ultimate tensile strain of the PFRP. For PFRP
 371 tube-PVC-RAC-RCBA specimens with different thicknesses of the PFRP tube, their failure
 372 modes were similar and had a single longitudinal crack in the PFRP-PVC tubes. No
 373 debonding between PFRP and PVC tubes was observed. In addition, apparent bulging of the
 374 PFRP-PVC tubes was observed, as illustrated in Fig. 13(d), (e) and (f). Thus, the increase in
 375 the PFRP thickness did not change the general failure mode of the PFRP-PVC-RAC-RCBA.
 376 For PFRP strip-PVC-RAC-RCBA specimens, the failure modes were different from the PFRP
 377 tube-PVC-RAC-RCBA. The PFRP-strip-PVC-RAC-RCBA specimens had circumferential
 378 cracks at the PVC tubes and the longitudinal cracks did not go through the whole height of the
 379 PFRP-strip-PVC tubes, as shown from Fig 13(g)-(l). The appearance of the hoop rupture at
 380 the PVC tubes attributed to the local strengthening effect of the PFRP strips on the PVC tubes.
 381 As can be further observed, the increase of the thickness of the PFRP strips and the change of
 382 the spacing of the PFRP strips did not change the failure modes of the PFRP strip-PVC-RAC-
 383 RCBA.

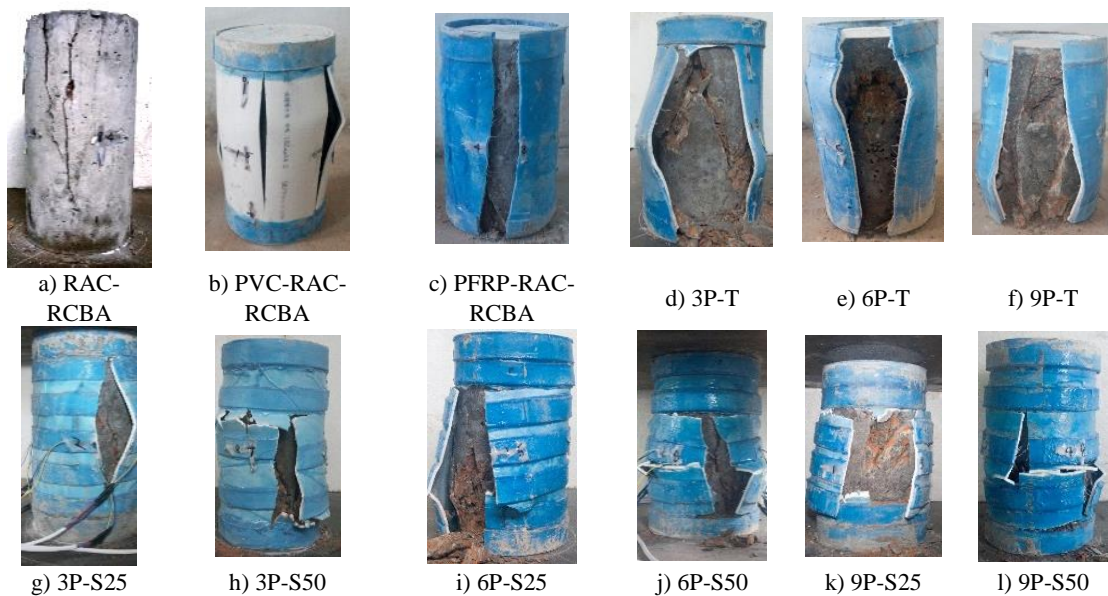


Fig.13 Failure modes of different confined RAC-RCBA specimens

384

385 3.2 Axial stress-strain behavior

386 3.2.1 The typical compressive stress-strain curves of PFRP-PVC-RAC-RCBA

387 The typical compressive stress-strain curves of unconfined RAC-RCBA, PVC-RAC-RCBA,
 388 6-layer PFRP-RAC-RCBA, 6-layer PFRP tube-PVC-RAC-RCBA, 6-layer 25 mm and 50 mm
 389 PFRP strip-PVC-RAC-RCBA specimens are illustrated in Fig 14. One representative
 390 compressive stress-strain curve obtained from one of the three specimens for each type of
 391 FRP confined RAC-RCBA specimens was used to plot the figure. For PVC-RAC-RCBA and
 392 PFRP-RAC-RCBA specimens, their curves can be characterized by two distinct stages: the
 393 first linear elastic response to the peak stress and followed by a nonlinear descending stage.
 394 No obvious transition zone between the first linear stage and the second non-linear stages can
 395 be found. In general, the stress-strain curve of PFRP-PVC-RAC-RCBA can be divided into
 396 three zones: the first linear elastic ascending stage close to the peak stress, the second distinct
 397 short non-linear ascending zone until the peak stress and the third non-linear descending stage
 398 after the peak stress. Fig 15 gives a schematic view of the compressive stress-axial strain
 399 curve for PFRP-PVC-RAC-RCBA specimens, which can be represented by two key points:

400 the transitional point (TP) corresponds to the peak stress point (i.e., peak stress f_{ct} and
 401 corresponding peak strain ϵ_{ct} point) and the ultimate point (UP) corresponds to the end of the
 402 curves at the ultimate state (i.e., ultimate strain ϵ_{cu} and corresponding ultimate stress f_{cu}).
 403 Unlike the traditional CFRP and GFRP confined RAC (e.g. when the CFRP and GFRP had a
 404 thickness of 4 and 6 layers in Ref. [21], where 4-layer and 6-layer GFRP-RAC and CFRP-
 405 RAC showed an ascending branch in the second stage of the compressive stress-strain curves)
 406 which showed a typical bilinear response with a linear and ascending stage after the transition
 407 zone, all the PFRP-RAC-RCBA, PVC-RAC-RCBA, and PFRP-PVC-RAC-RCBA showed
 408 the descending stages at the second stage. In the other words, the ultimate strain does not
 409 happen at the peak stress point but develops until the failure of specimens due to the ductility
 410 of materials [38]. Therefore, the PFRP-RAC-RCBA, PVC-RAC-RCBA and PFRP-PVC-
 411 RAC-RCBA specimens can be defined as weakly-confined specimens, although enhancement
 412 in compressive strength and ductility were obtained.

413

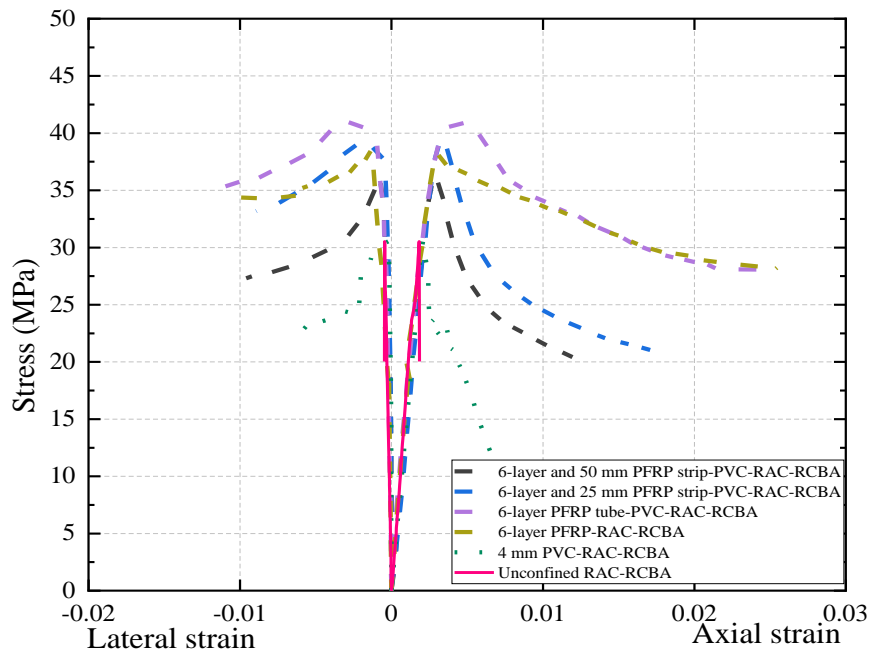


Fig.14 Stress-strain curves of different confinement modes

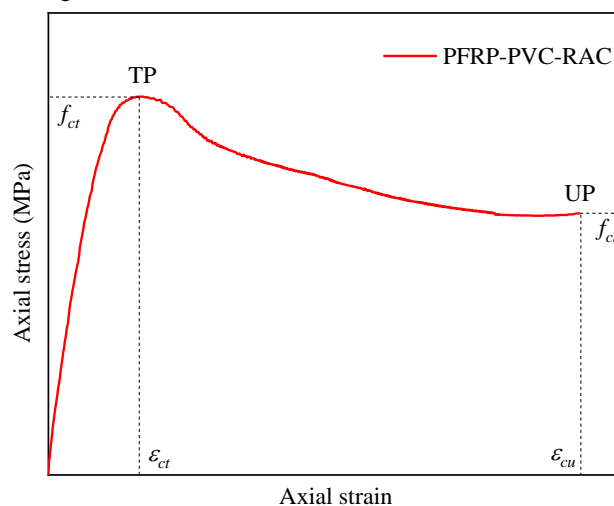


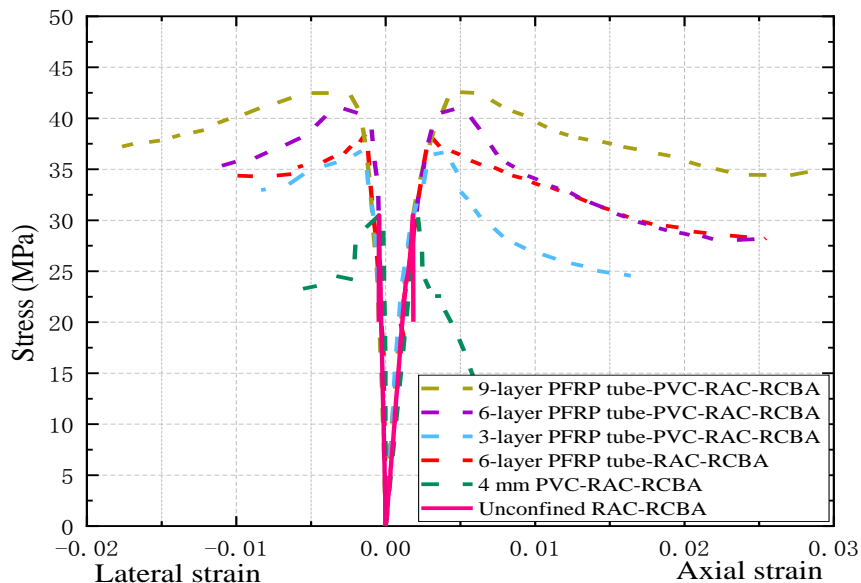
Fig.15 Typical axial compressive stress-strain curves of PFRP tube-PVC-RAC-RCBA and PFRP strip-PVC-RAC-RCBA

414 3.2.2 The influence of confinement types on compressive stress-strain behavior

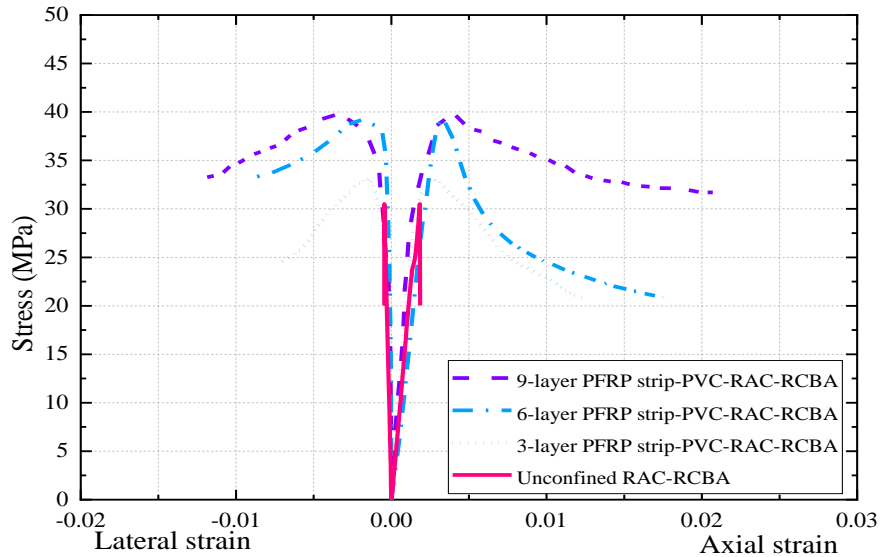
415 The overall patterns of the stress-strain behaviors of PFRP-RAC-RCBA, 6-layer PFRP tube-
 416 PVC-RAC-RCBA and 6-layer PFRP strip-PVC-RAC-RCBA with spacing distances of 25
 417 and 50 mm illustrated in Fig. 14 are similar, which consisted of three stages: the initial elastic
 418 linear ascending stage, the second nonlinear ascending stage and the final descending stage.
 419 The PVC-RAC-RCBA specimens showed steeper descending stage and less peak stress than
 420 PFRP-RAC-RCBA, PFRP strip-PVC-RAC-RCBA and PFRP tube-PVC-RAC-RCBA
 421 specimens, but less slope of descending stage than that of the plain RAC-RCBA. The stress-
 422 strain curve of 6-layer PFRP-RAC-RCBA exhibited a sharper turning point from the peak
 423 stress point to the descending stage and larger slope of the descending stage than those of 6-
 424 layer PFRP tube-PVC-RAC-RCBA specimens. While the ultimate strains at UP point of 6-
 425 layer PFRP-RAC-RCBA were like those of 6-layer PFRP tube-PVC-RAC-RCBA but the
 426 peak stress at TP point of 6-layer PFRP-RAC-RCBA was lower than that of 6-layer PFRP
 427 tube-PVC-RAC-RCBA and was close to that of 6-layer and 25 mm spacing distance PFRP
 428 strip-PVC-RAC-RCBA. The stress-strain curves of 6-layer PFRP strip-PVC-RAC-RCBA
 429 presented obviously more steep descending stage than that of 6-layer PFRP tube-PVC-RAC-
 430 RCBA, and the ultimate axial strain and peak stress of 6-layer PFRP strip-PVC-RAC-RCBA
 431 were less than those of 6-layer PFRP tube-PVC-RAC-RCBA.

432 3.2.3 The influence of PFRP thickness on stress-strain behavior

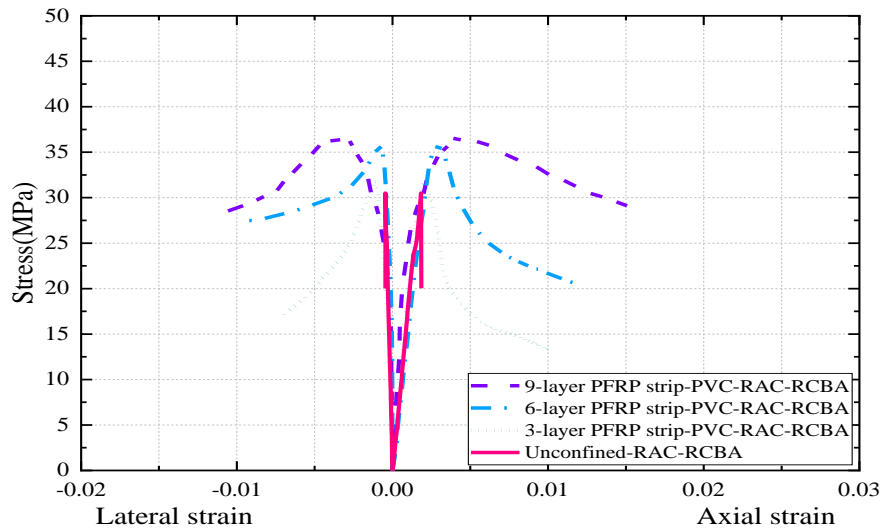
433 According to Fig. 16(a), the stress-strain behavior of PFRP tube-PVC-RAC-RCBA showed a
 434 little steeper trend at the second ascending stages with a decrease of PFRP thickness and more
 435 placid descending stages with an increase of PFRP thickness, and the TP points performed
 436 gentler transition with an increase of PFRP thickness. The stress-strain curves of PFRP strip-
 437 PVC-RAC-RCBA of the same spacing distance of PFRP strip in Fig. 16 (b) and (c) exhibited
 438 similar trend to those of PFRP tube-PVC-RAC-RCBA that the initial ascending stages were
 439 coincided with that of plain RAC-RCBA, the slopes of the second ascending stages became
 440 lower and the descending stages turn more placid with an increase of PFRP thickness. The
 441 ultimate strains at UP point and peak stress at TP point were higher for all PFRP-PVC-RAC-
 442 RCBA specimens with an increase of PFRP thickness.



a) PFRP tube



b) PFRP strip with spacing of 25 mm



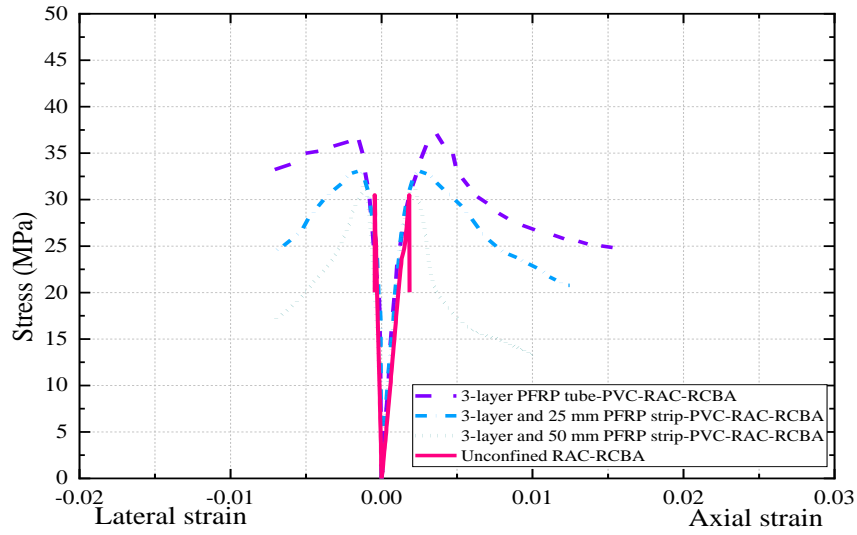
c) PFRP strip with spacing of 50 mm

Fig.16 Stress-strain curves of different PFRP layers-PVC confined RAC-RCBA cylinders

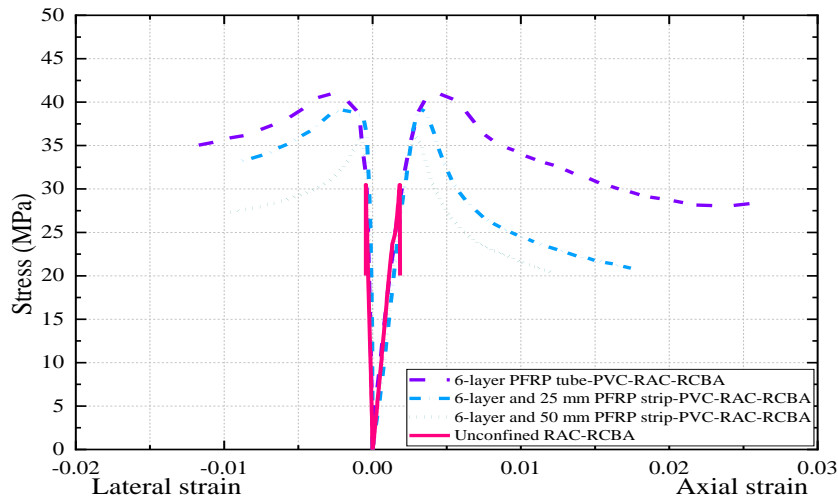
443

444 *3.2.4 The influence of spacing distance of PFRP strip on stress-strain behavior*

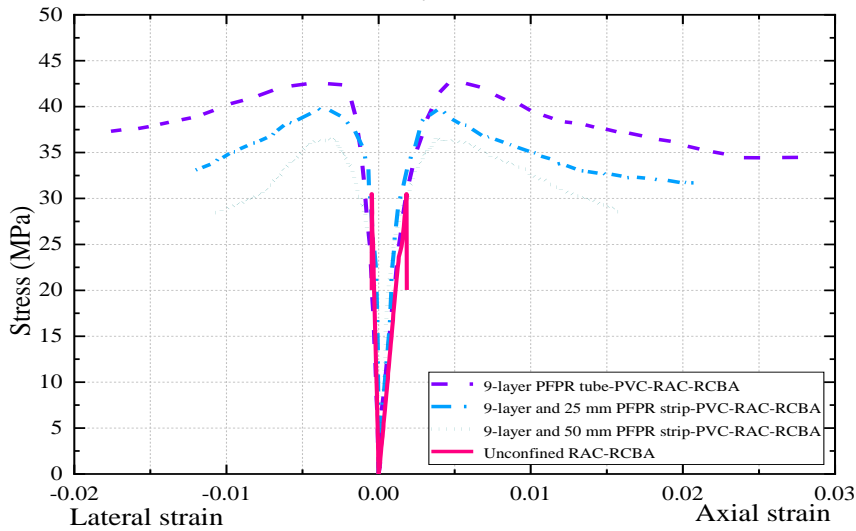
445 The stress-strain curves in Fig. 17 present similar trend with different spacing distances of
 446 PFRP strip to the typical stress-strain behavior in Fig. 15. The ascending stages of 3-layer and
 447 6-layer PFRP strip-PVC-RAC-RCBA groups exhibited the similar slope with different
 448 spacing distance of PFRP strip while the slopes of the descending stages became lower with a
 449 decrease of spacing distance of PFRP strip. For 9-layer PFRP strip-PVC-RAC-RCBA group,
 450 the slopes of the second ascending stages increased obviously with a decrease of spacing
 451 distance of PFRP strip, besides the descending stages showed more placid with a decrease of
 452 spacing distance of PFRP strip. For all PFRP strip-PVC-RAC-RCBA specimens, the ultimate
 453 strains at UP point and peak stress at TP point increased with a decrease of spacing distance
 454 of PFRP strip.



a) 3-layer PFRP



b) 6-layer PFRP



c) 9-layer PFRP

Fig.17 Compressive stress-strain curves of different spacing distance of PFRP strip-PVC confined RAC-RCBA cylinders

455

456 **3.3 Discussion on tested results**

457 **3.3.1 Load carrying capacity and ductility analysis**

458 All the tested results are listed in Table 6, where f_{co} and ε_{co} are the peak stress and
 459 corresponding axial strain of unconfined RAC-RCBA, respectively, f_{ct} and ε_l , ε_{ct} are the
 460 peak stress, corresponding lateral and axial strain of confined specimens, f_{cu} and ε_{cu} are the
 461 ultimate stress and corresponding ultimate axial strain of the confined specimens. The lateral
 462 confining pressure f_l is calculated as Eq. (1) [21], where the f_{frp} and t_{frp} are the tensile strength
 463 and thickness of the FRP or PVC, respectively, d is the diameter of the concrete cylindrical
 464 specimens.

$$f_l = 2f_{frp}t_{frp}/d \quad (1)$$

466

Table 6 Tested results

Specimen	f_{co} (MPa)	ε_{co} (10^{-2})	f_{ct} (MPa)	ε_{ct} (10^{-2})	ε_l (10^{-2})	f_l (MPa)	f_{cu} (MPa)	ε_{cu} (10^{-2})
RAC-RCBA	30.6	0.2	—	—	—	—	—	—
PVC-RAC-RCBA	30.6	0.2	30.6	0.21	0.02	1.20	6.4	0.79
PFRP-RAC-RCBA	30.6	0.2	38.4	0.30	0.14	2.31	28.2	2.55
3P-T	30.6	0.2	37.1	0.36	0.18	2.32	24.5	1.64
3P-S25	30.6	0.2	33.1	0.26	0.16	1.64	20.8	1.25
3P-S50	30.6	0.2	31.9	0.21	0.12	1.44	13.3	1.00
6P-T	30.6	0.2	40.9	0.45	0.28	3.73	28.3	2.54
6P-S25	30.6	0.2	39.3	0.34	0.21	2.21	20.9	1.75
6P-S50	30.6	0.2	36.0	0.29	0.08	1.78	20.4	1.20
9P-T	30.5	0.2	42.6	0.50	0.32	5.17	34.7	2.84
9P-S25	30.5	0.2	39.8	0.41	0.40	2.79	31.7	2.02
9P-S50	30.5	0.2	36.5	0.38	0.30	2.12	28.4	1.59

467

468 According to the tested results, the increments in the compressive strength enhancement at TP
 469 point in Fig. 15 by the different confinements can be calculated. The corresponding increase
 470 ratios of different confined RAC-RCBA referring to the unconfined RAC-RCBA can be
 471 obtained and are listed in Fig.18 which shows that the PVC tube confinement did not provide
 472 enhancement in the compressive strength of the RAC-RCBA, which may be attributed to the
 473 very low confining pressure provided by the PVC tube, as listed in Eq. (1), the lateral
 474 confining pressure is high dependent on the tensile strength and the thickness of the PVC,
 475 both of which are relatively small. The 6-layer PFRP tube confinement resulted in a 26%
 476 increase in the compressive strength of the RAC-RCBA. Overall, both PFRP tube-PVC and
 477 PFRP strip-PVC confinement enhanced the compressive strength of RAC-RCBA effectively.
 478 Comparison of PFRP tube-PVC-RAC-RCBA with different thickness of PFRP tube (i.e., 3P-
 479 T, 6P-T and 9P-T) demonstrated that with an increase of number of the PFRP layers, the
 480 increment of compressive strength of the RAC-RCBA enhanced. For PFRP strip-PVC-RAC-
 481 RCBA specimens with the same strip thickness but different strip spacing (i.e., 3P-S25 and
 482 3P-S50, 6P-S25 and 6P-S50, 9P-S25 and 9P-S50), increasing the spacing distance of the
 483 PFRP strip reduced the increments to some extent. Besides, the PFRP tube-PVC-RAC-RCBA
 484 had larger compressive strength than the corresponding PFRP strip-PVC-RAC-RCBA with
 485 the same PFRP and PVC thickness.

486

487 The ductility indices μ of all the confined specimens in Fig. 19 were calculated as the ratio of
 488 the ε_{cu} to the ε_{co} . The PVC-RAC-RCBA showed an obvious improvement in the ductility,
 489 which was 4.2. The 6-layer PFRP-RAC-RCBA also had a significantly enhanced ductility
 490 index, which was 13.4. Comparison of PFRP tube-PVC-RAC-RCBA (i.e., 3P-T, 6P-T and
 491 9P-T) with different PFRP tube thicknesses demonstrated that with an increase of number of
 492 the PFRP layers, the ductility index also increased remarkably. In general, the ductility index
 493 of the PFRP tube-PVC-RAC-RCBA specimen was larger than that of the corresponding

494 PFRP strip-PVC-RAC-RCBA with the same thickness of PFRP. For the PFRP strip-PVC-
 495 RAC-RCBA specimens, an increase in the PFRP strip thickness also increased the ductility
 496 index remarkably and an increase in the strip spacing reduced the inductility index of the
 497 specimen. It should be pointed out here that the comparison in strength and ductility index is
 498 based on the limited number of replications and the percentage increments are based on the
 499 comparison on average values of tested group.

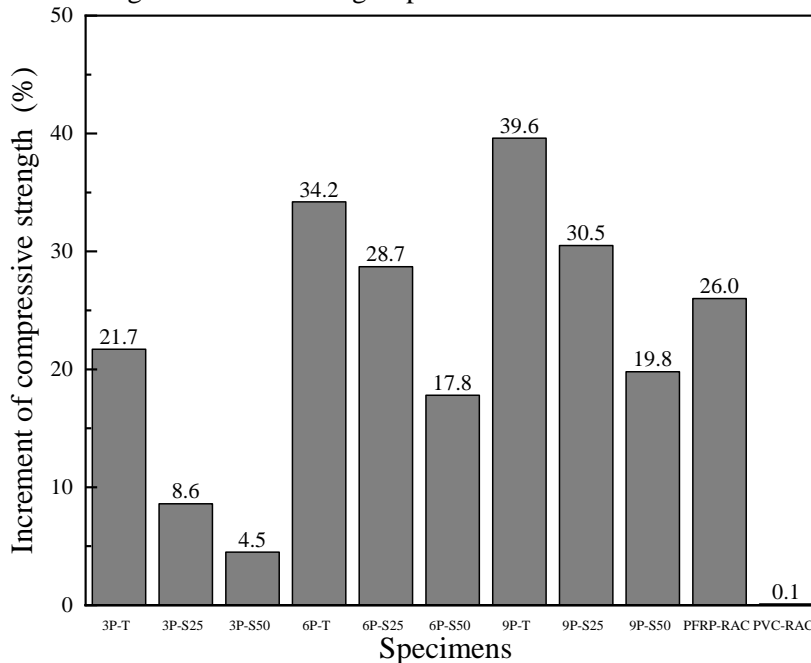


Figure 18: Increment ratios of compressive strength of different confined RAC-RCBA specimens

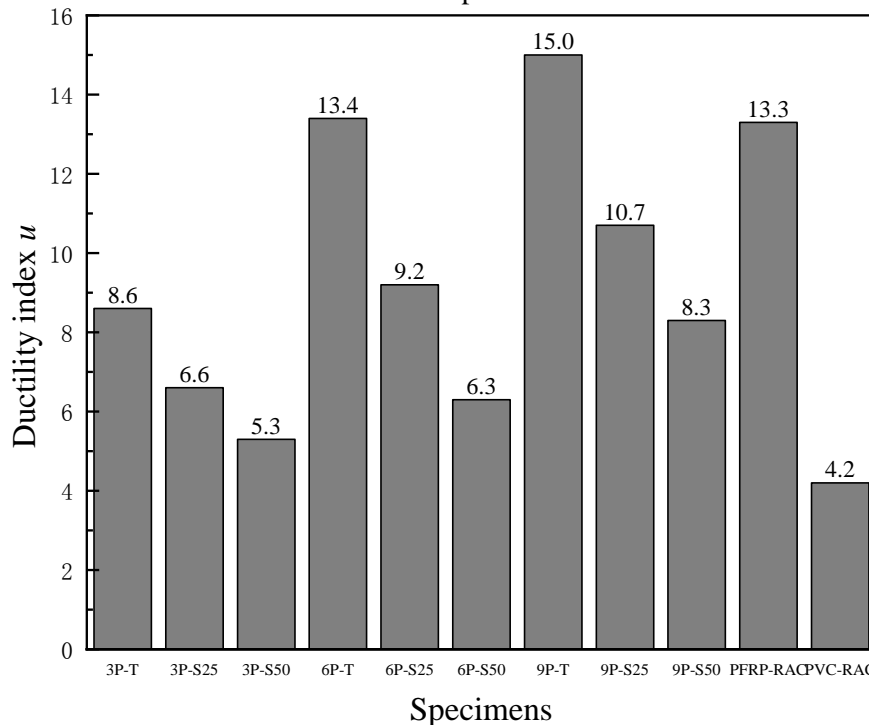


Figure 19. Ductility indexes of the confined specimens

500 3.3.2 Comparison with GFRP-RAC-RCBA and CFRP-RAC-RCBA

501 In this section, the results of current study were compared with those of GFRP tube encased
 502 and CFRP tube encased RAC-RCBA specimens in Ref. [21]. The compressive strength of the

503 unconfined RAC-RCBA, the replacement ratio of RAs for the RAC-RCBA, the constitutive
 504 of the RAs, and the size of the RAC-RCBA used in Ref. [21] were similar as those used in
 505 current study. The comparison in results of 6-layer CFRP-RAC-RCBA, 6-layer GFRP-RAC-
 506 RCBA, 6-layer PFRP-RAC-RCBA and 6-layer PFRP tube-PVC-RAC-RCBA is listed in
 507 Table 7. The comparison in the tensile properties of PFRP, PVC, GFRP and CFRP can be
 508 found in Table 5.

509
 510 The comparison indicated that the 6-layer CFRP or 6-layer GFRP tube encased RAC-RCBA
 511 had much higher compressive strength than that of 6-layer PFRP-RAC-RCBA or 6-layer
 512 PFRP tube-PVC-RAC-RCBA, while the ductility indices of 6-layer CFRP-RAC-RCBA and
 513 6-layer GFRP-RAC-RCBA were much lower than that of the 6-layer PFRP-RAC-RCBA or
 514 6-layer PFRP-PVC-RAC-RCBA. The confinement ratio is defined as f_{cu}/f_{co} to evaluate the
 515 effectiveness of FRP confinement on concrete, and the ratios of confinement ratio and cost
 516 were calculated to compare the cost performance as Table 7. Although the confinement ratios
 517 of PFRP-RAC-RCBA and PFRP tube-RAC-RCBA are lower than those of CFRP-RAC-
 518 RCBA and GFRP-RAC-RCBA, the ratios of confinement ratio and cost of PFRP-RAC-
 519 RCBA and PFRP tube-PVC-RAC-RCBA are much higher than those of CFRP-RAC-RCBA
 520 and GFRP-RAC-RCBA.

521
 522

Table 7 Comparison of CFRP, GFRP and PFRP tube confined RAC-RCBA

Specimens	f_{co} (MPa)	ε_{co} (%)	f_{cu} (MPa)	ε_{cu} (%)	μ	f_l (MPa)	f_l/f_{co}	f_{cu}/f_{co}	Price of fibers (RMB/m ²)	Confinement ratio/Cost
6L-CFRP- RAC-RCBA	33.3	0.3	161.3	1.71	5.6	40.7	1.22	4.84	Glass fibre 80	0.61
6L GFRP- RAC-RCBA	33.3	0.3	148.6	2.28	7.7	33.3	1	4.46	Carbon fibre 160	0.07
6L PFRP- PVC-RAC- RCBA	30.5	0.2	40.9	2.54	13.4	3.7	0.12	1.34	Polyester fibre 1.1	1.22
6L PFRP- RAC-RCBA	30.5	0.2	38.4	2.55	13.3	3.2	0.10	1.26	Polyester fibre 1.1	1.14

523

524 3.4 Dilation behavior

525 In this section, the discussion on the dilation behavior of PFRP-PVC-RAC-RCBA specimens
 526 is presented. The dilation effect was caused by the expansion of the core concrete when the
 527 applied stress was close to or exceeded the ultimate axial stress of the concrete and then the
 528 outer confining tubes were activated to dilate. The dilation rate μ_t is expressed as the slope of
 529 the lateral strain increment to axial strain increment and given as Eq. (2) [67]. The
 530 corresponding dilation rates of PFRP-PVC-RAC-RCBA are presented in Fig.20.

$$531 \mu_t = \Delta\varepsilon_h / \Delta\varepsilon_c \quad (2)$$

532 As illustrated in Fig.20, the peak dilation rate of PVC-RAC-RCBA is considerable indicating
 533 the significant improvement in ductility due to the PVC confinement (as illustrated in Fig 19).
 534 The peak dilation rate of the 6-layer PFRP-RAC-RCBA is like that of 6-layer PFRP tube-
 535 RAC-RCBA. For PFRP tube-PVC-RAC-RCBA with different PFRP thicknesses (i.e., 3P, 6P
 536 and 9P), both the ultimate axial strains and the peak dilation rates increase with an increase of
 537 the PFRP thickness. For PFRP strip-PVC-RAC-RCBA with different strip spacing (i.e., 3P-
 538 S25 and 3P-S50, 6P-S25 and 6P-S50, 9P-S25 and 9P-S50), a decrease of spacing distance of
 539 the PFRP strip enhances the peak dilation rate with more ductile characteristic of specimens.
 540 In addition, the PFRP tube-PVC-RAC-RCBA specimens always present larger dilation rate
 541 than the corresponding PFRP strip-PVC-RAC-RCBA specimens with the same PFRP
 542 thickness.

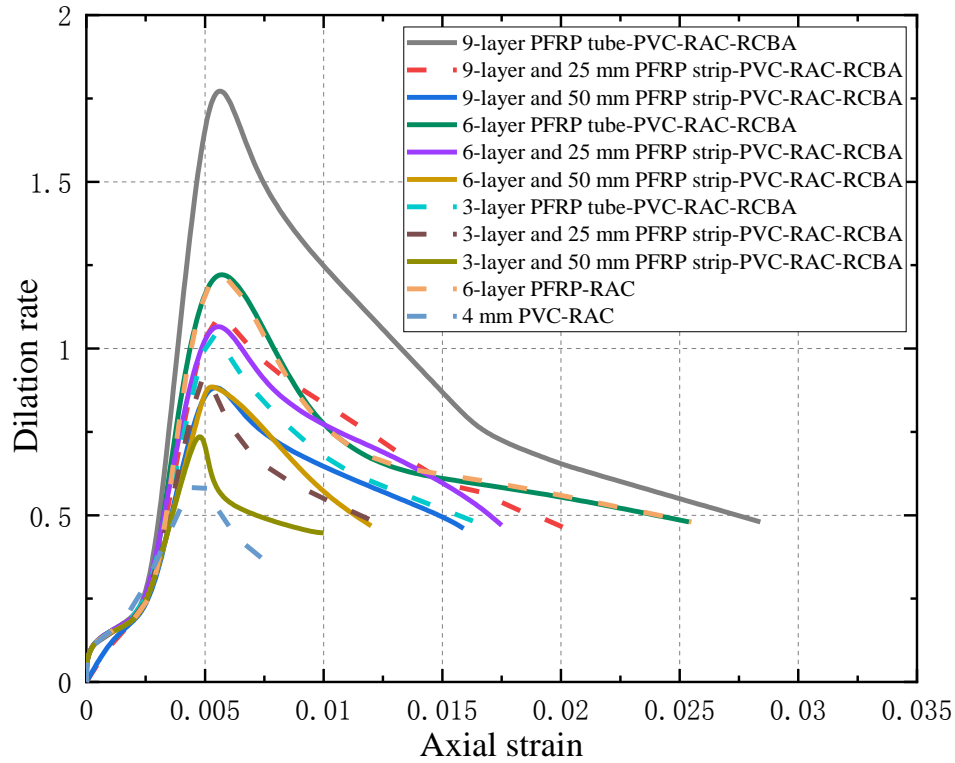
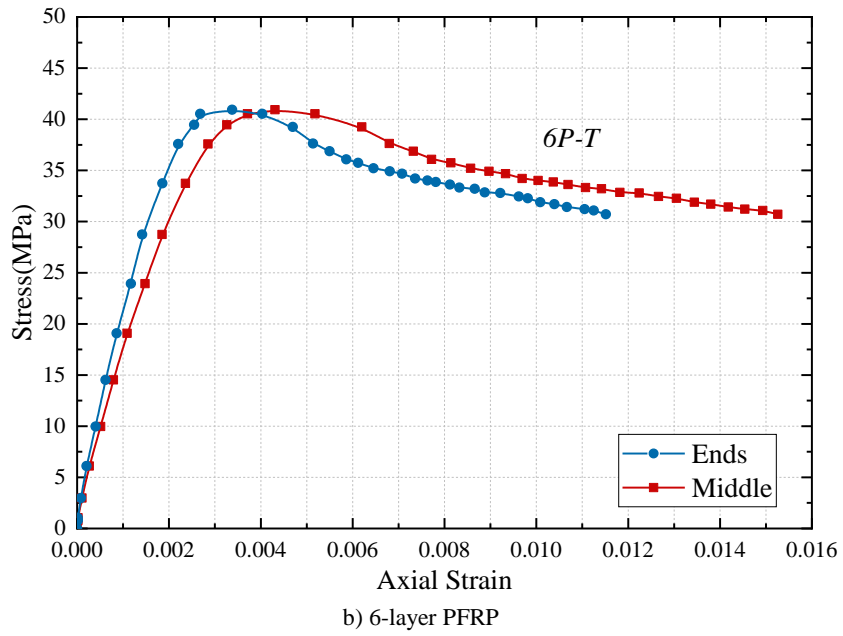
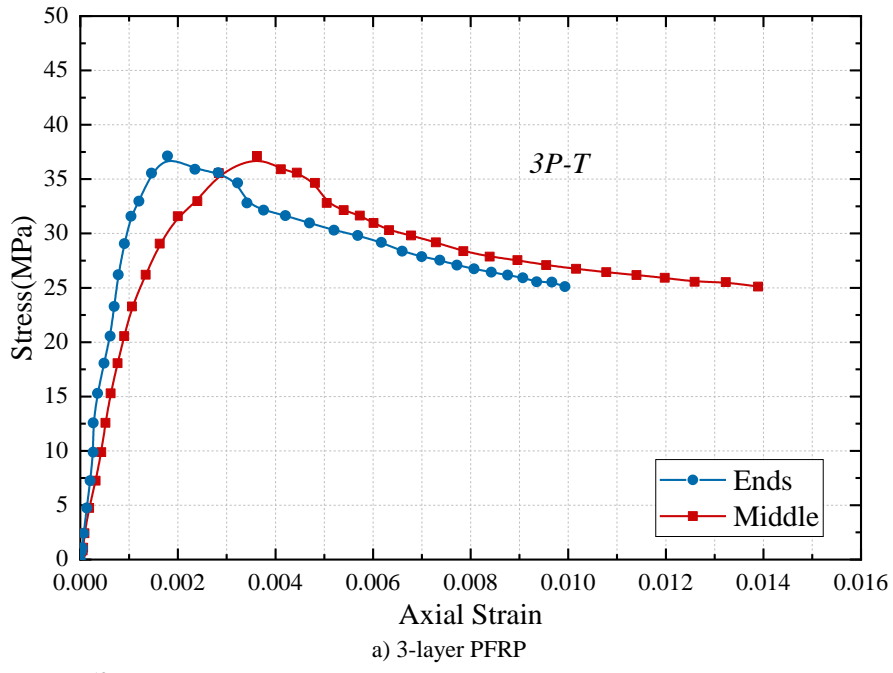


Fig.20 Dilation rates of PFRP-PVC-RAC-RCBA specimens

543 **3.5 Axial strain at mid height and ends of the tubes**

544 The average axial strains at the mid height and ends of the PFRP tube-PVC-RAC-RCBA
545 specimens (i.e., 3P-T 6P-T and 9P-T specimens) were obtained from the four strain gauges at
546 the mid height on the surface of the PFRP tube (i.e., SG5, SG6, SG7 and SG8, see Fig 12) and
547 four axial strain gauges at both the ends at the surface of the PFRP tube (i.e., SG9, SG10,
548 SG11 and SG12, see Fig 12). The comparisons of the stress and axial strain at the mid height
549 and both ends of specimens (i.e., 3P-T, 6P-T and 9P-T) are shown in Fig. 21. Generally, the
550 overall tendency of the stress-strain behavior at the middle region of specimens is similar to
551 that at the ends of specimens. Apparently, the axial deformation at the middle region of
552 specimens is larger than that at the ends of specimens under the same stress. The possible
553 reasons include: (1) the larger expansion of core concrete at the middle region under the
554 compression, and (2) the existing of two extra PFRP strip strengthening at both the ends of
555 specimens in order to avoid premature rupture of ends of specimens. The difference in the
556 axial strain between the mid-height and ends of specimens was more pronouncedly for
557 specimens with less thick of the PFRP tube.



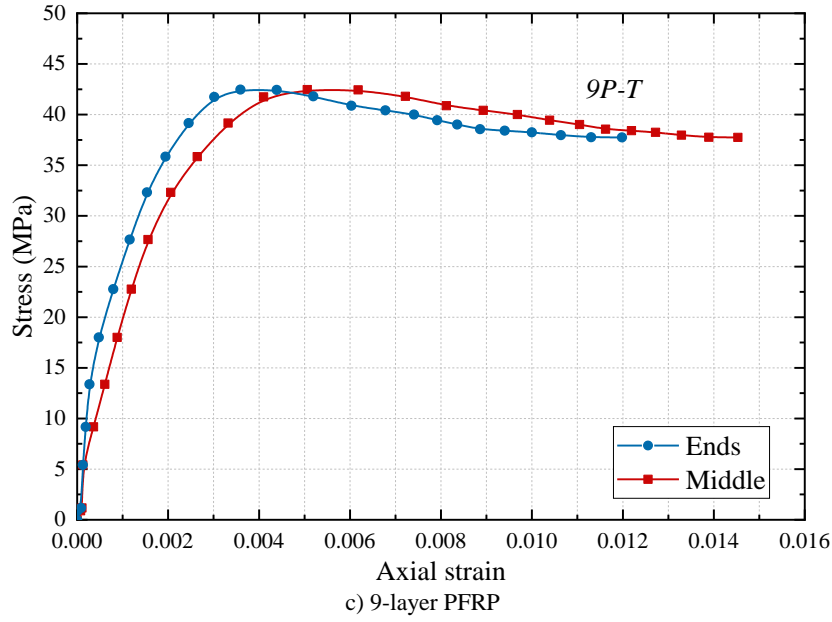


Fig.21 End and middle stress-strain curves of PFRP tube-PVC- RAC-RCBA cylinders

558 4 Analytical modeling of PFRP-PVC-RAC-RCBA

559 4.1 Mechanical characteristics analysis of PFRP-PVC-RAC-RCBA in compression

560 For the purpose of designing PFRP-PVC-RCBA-RCBA structures for practical application,
 561 accurate stress-strain models should be developed. To develop stress-strain models, it is
 562 important for us to understand the mechanical characteristics of PFRP-PVC-RAC-RCBA in
 563 axial compression. In this study, the mechanical characteristics analysis of PFRP-PVC-RAC-
 564 RCBA in axial compression followed the mechanical analysis of FRP-steel tube confined
 565 concrete introduced by Teng et al. [60]. With the similar analysis, the mechanical
 566 characteristics of PFRP-PVC-RAC-RCBA in axial compression can be obtained and is
 567 illustrated in Fig.22. The core concrete is under a tri-axial compression state, therefore the
 568 load carrying capacity and deformation capacity of the concrete are enhanced. From Fig. 22,
 569 it is clear that both PFRP and the PVC provided the lateral confining pressure to the concrete
 570 core, as expressed by Eq. (3):

$$571 \quad f_l' = f_{lf} + f_{lp} \quad (3)$$

572 As shown in Fig 22(b), the force equilibrium in the PVC tube can be expressed by Eq. (4):

$$573 \quad f_{lp} = \frac{2E_{pvc}\varepsilon_{pvc}t_{pvc}}{d} \quad (4)$$

574 As shown in Fig 22(a), the force equilibrium in the PFRP section can be expressed by Eq. (5):

$$575 \quad f_{lf} = \frac{2E_{frp}\varepsilon_{frp}t_{frp}}{d+2t_{pvc}} \quad (5)$$

576 Where f_l' is the lateral confining pressure of the composite confinement on concrete core, f_{lf} is
 577 the effective lateral confining pressure provided by PFRP, f_{lp} is lateral confining pressure
 578 provided by PVC, E_{pvc} , ε_{pvc} , and t_{pvc} are the elastic modulus, tensile strain in the hoop direction
 579 and thickness of the PVC tube, E_{frp} , ε_{frp} , and t_{frp} are the elastic modulus, tensile strain in the
 580 hoop direction and thickness of PFRP tube, d is the diameter of the core concrete.

581 For PFRP strip-PVC-RAC-RCBA cylinders, the equivalent PFRP thickness t_{frp}' can be written
 582 by Eq.(6):

$$583 \quad t_{frp}' = \frac{nb_{frp}}{H} t_{frp} \quad (6)$$

584 Then, the force equilibrium of the PFRP strip confinement can be written as following Eq.(7)::

$$585 \quad f_{lf} = \frac{2nE_{frp}\varepsilon_{frp}b_{frp}t_{frp}}{H(d+2t_{pvc})} \quad (7)$$

586 Where n is the number of PFRP strips, b_{frp} is the width of PFRP strip, H is the height of
 587 concrete cylinders. The lateral confining pressure provided by the PFRP strips was imposed
 588 onto the concrete core through the PVC to, the dispersion angle was 45° and the dispersion

589 width was the thickness of the PVC tube (Fig 23), as explained by Teng et al. [65]. Thus, the
 590 effective lateral confining pressure onto the concrete core can be expressed by

$$591 \quad f'_{lf} = k_e f_{lf} \quad (8)$$

$$592 \quad k_e = \frac{A_e}{A} \quad (9)$$

$$593 \quad A_e = A - m \frac{(s-2t_{pvc})^2}{2} \quad (10)$$

$$594 \quad A = dH \quad (11)$$

595 Where k_e is the effective confining coefficient of the PFRP strip, and $k_e = 1$ is for PFRP tube
 596 confinement, A_e is the effective confining area of the core concrete, A is the gross area of
 597 specimens including the core concrete and external hybrid tube, m is the number of zone
 598 without confinement among PFRP strip, s is the spacing distance of the PFRP strip. Overall,
 599 the Eq.(3) can be expressed as Eq.(12):

$$600 \quad f'_l = f'_{lf} + f_{lp} = k_e f_{lf} + f_{lp} \quad (12)$$

601 Specifically, for PFRP tube-PVC-RAC-RCBA cylinders:

$$602 \quad f'_l = \frac{2E_{frp}\varepsilon_{frp}t_{frp}}{d+2t_{pvc}} + \frac{2E_{pvc}\varepsilon_{pvc}t_{pvc}}{d} \quad (13)$$

603 For PFRP strip-PVC-RAC-RCBA cylinders:

$$604 \quad f'_l = k_e \frac{2nE_{frp}\varepsilon_{frp}t_{frp}}{H(d+2t_{pvc})} + \frac{2E_{pvc}\varepsilon_{pvc}t_{pvc}}{d} \quad (14)$$

605

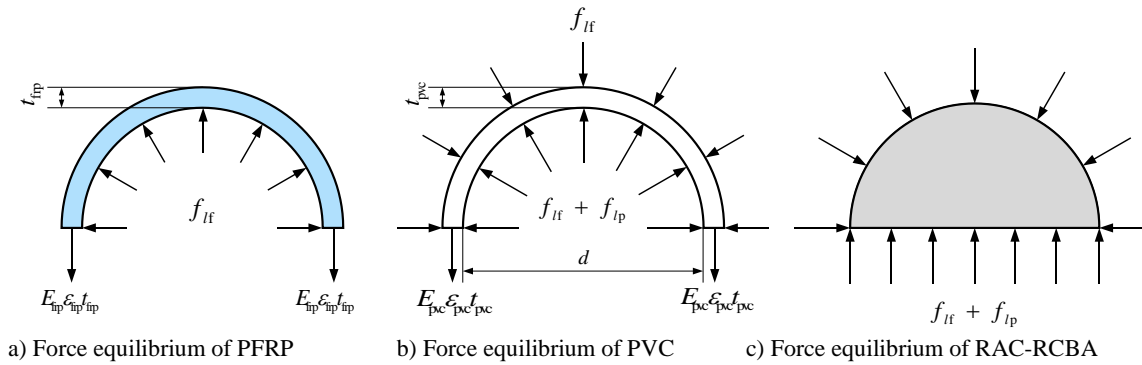


Fig.22 Mechanical characteristics of PFRP tube-PVC-RAC-RCBA cylinder

606

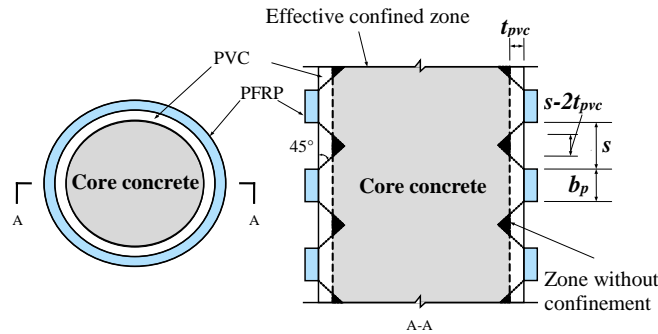


Fig.23 Mechanical characteristics of PFRP strip-PVC-RAC-RCBA cylinder

607 **4.2 Strength and corresponding strain models for PFRP-PVC-RAC-RCBA specimens**

608 The discussion in Section 3.3 shows that the RAC-RCBA cylinders were weakly-confined by
 609 the PFRP-PVC tube although remarkably enhancement in compressive strength and ductility
 610 were achieved. That is to say, the strain of PFRP-PVC-RAC-RCBA at peak stress at TP point
 611 in Fig.15 (i.e., compressive strength) point named peak strain was not the ultimate strain of
 612 PFRP-PVC-RAC-RCBA (i.e., UP point in Fig.15) where the hybrid confined system failed.
 613 Generally, the ultimate stress and ultimate strain were related to the elastic modulus of
 614 confined materials and core concrete [62], in order to fit the strength model, the eigenvalue λ

615 was cited as Eq.(15) [62] for better expressing the relationship of ultimate stress and the
 616 elastic modulus of confined materials and core concrete:

$$617 \quad \lambda = \frac{E_l}{E_c} \quad (15)$$

618 Where E_c is the elastic modulus of the RAC-RCBA which is related to the square root of
 619 compressive strength $\sqrt{f_{co}}$ [61, 62] as Eq.(16), E_l is the effective lateral confining stiffness of
 620 the hybrid PFRP-PVC tube which is expressed as Eq.(17) and Eq.(18):

$$621 \quad \lambda = \frac{E_l}{\sqrt{f_{co}}} \quad (16)$$

$$622 \quad E_l = \frac{2E_{frp}t_{frp}}{d+2t_{PVC}} + \frac{2E_{PVC}t_{PVC}}{d} \quad (\text{For PFRP tube-PVC-RAC-RCBA}) \quad (17)$$

$$623 \quad E_l = k_e \frac{2nE_{frp}t_{frp}}{H(d+2t_{PVC})} + \frac{2E_{PVC}t_{PVC}}{d} \quad (\text{For PFRP strip-PVC-RAC-RCBA}) \quad (18)$$

624 The strength f_{cc}' and corresponding strain ε_{cc}' could be calculated as:

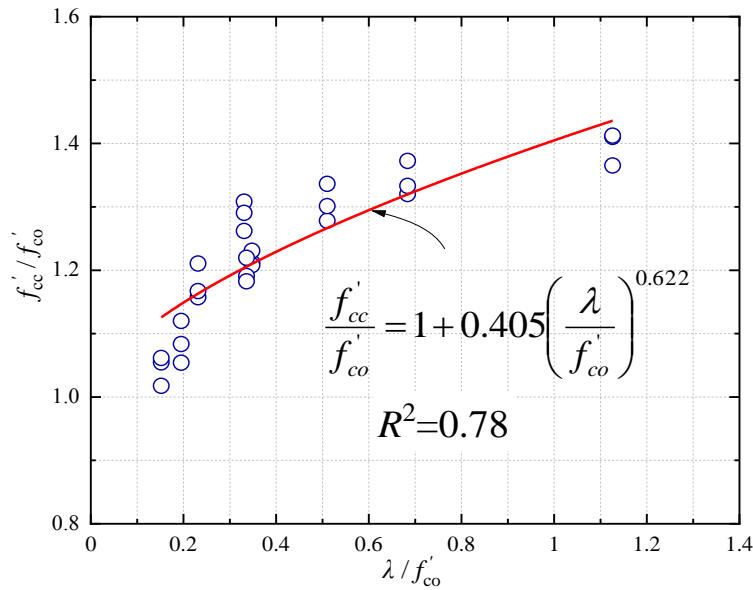
$$625 \quad \frac{f_{cc}'}{f_{co}} = 1 + k_1 \left(\frac{\lambda}{f_{co}} \right)^\alpha \quad (19)$$

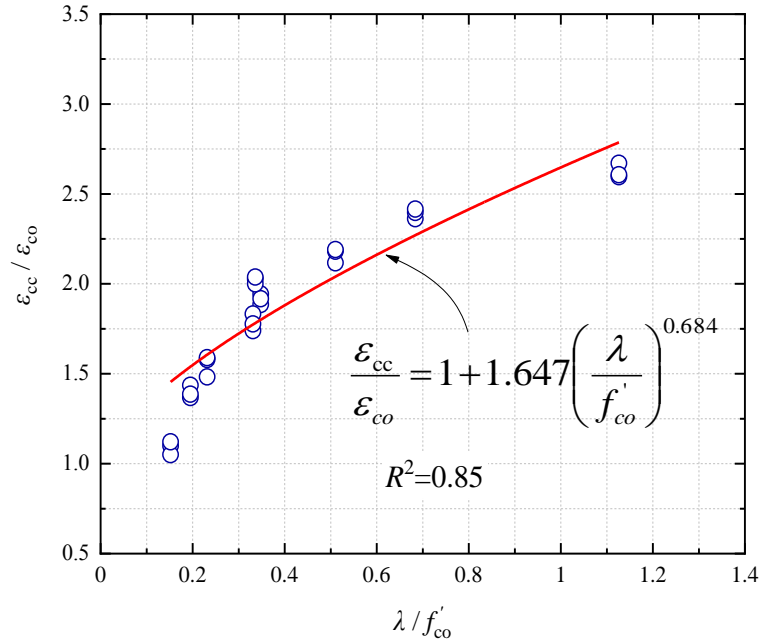
$$626 \quad \frac{\varepsilon_{cc}'}{\varepsilon_{co}} = 1 + k_2 \left(\frac{\lambda}{\varepsilon_{co}} \right)^\beta \quad (20)$$

627
 628 Based on the regression analysis and iterative computations of the tested results, the fitting
 629 coefficients $\alpha=0.622$ and $k_1=0.405$, $\beta=0.684$ and $k_2=1.647$ can be determined to create the
 630 strength and strain equations for PFRP-PVC-RAC-RCBA, as illustrated in Fig 24. The
 631 strength and peak strain models for PFRP-PVC-RAC-RCBA can be expressed by Eq.(21) and
 632 (22):

$$633 \quad \frac{f_{cc}'}{f_{co}} = 1 + 0.405 \left(\frac{\lambda}{f_{co}} \right)^{0.622} \quad (21)$$

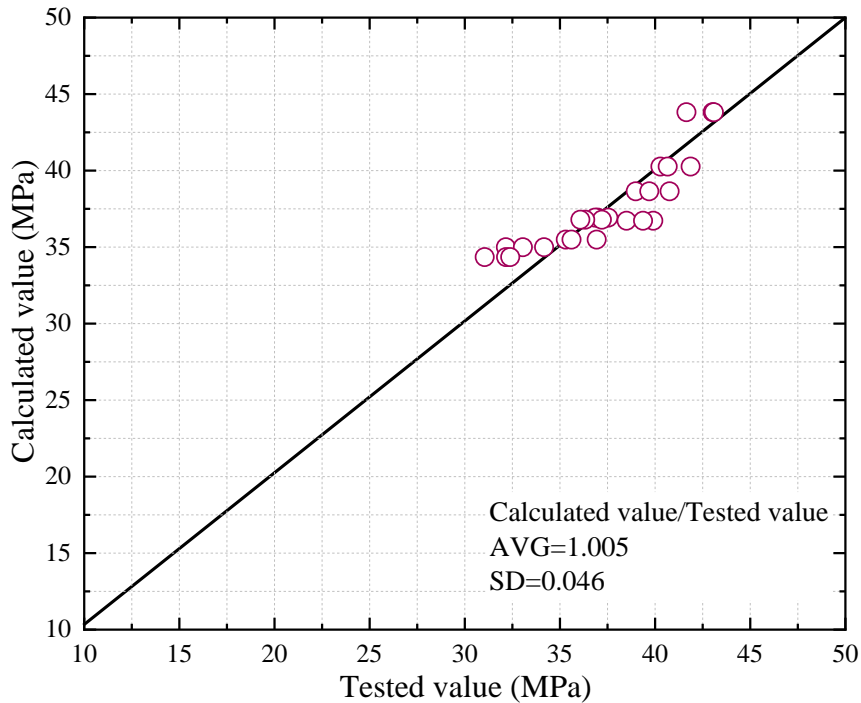
$$634 \quad \frac{\varepsilon_{cc}'}{\varepsilon_{co}} = 1 + 1.647 \left(\frac{\lambda}{\varepsilon_{co}} \right)^{0.684} \quad (22)$$



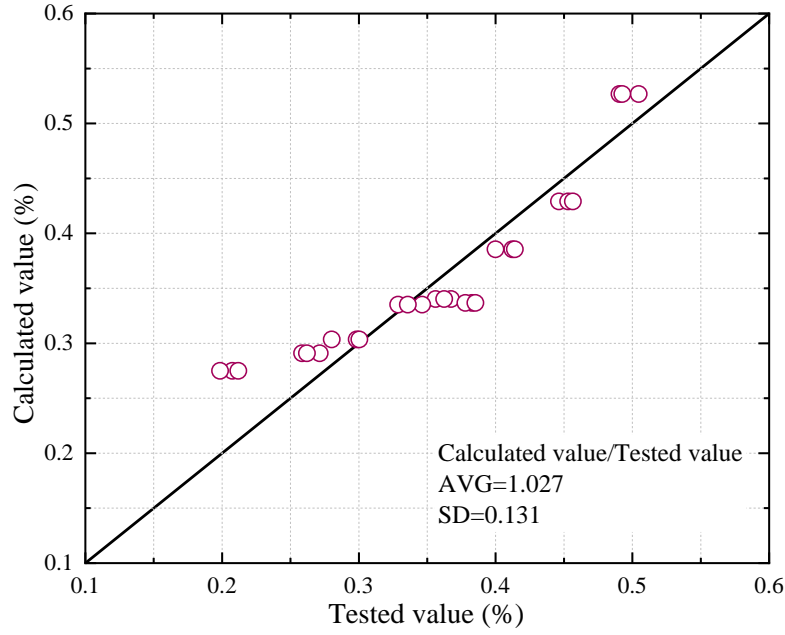


b) Fitting curves of peak strain model
 Fig. 24 Fitting curves of peak strength models

Based on the stress and strain equations above, the comparison in the peak strength and the peak axial strain between the experimental and predictions is shown in Fig 25. It can be seen that the predictions based on the developed stress and strain models matched the experimental stress and strain values of the PFRP-PVC-RAC-RCBA well, with relatively small deviations.



a) Performance of strength model



b) Performance of peak strain model

Fig. 25 Performance of peak strength models: strength and peak strain models

635 **4.3 Ultimate strain and corresponding stress models**

636 In literature, the ultimate strain and corresponding stress models for FRP confined concrete
 637 typically had the following expressions [63, 64]:

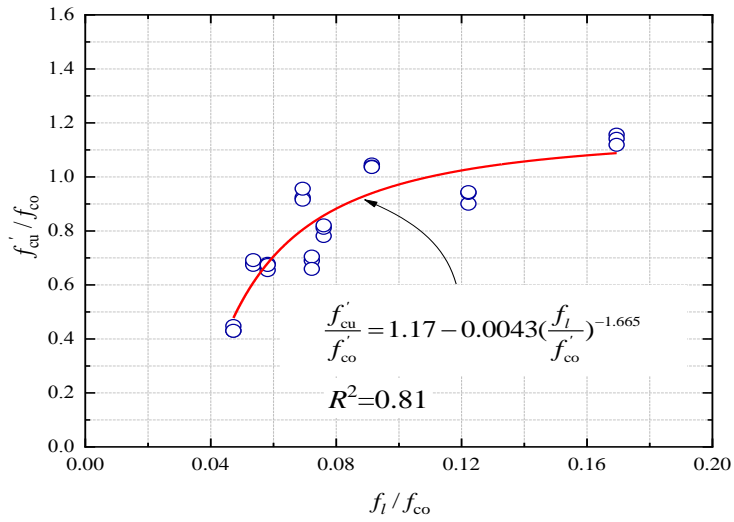
638
$$\frac{f'_{cu}}{f_{co}} = c_1 + k_3 \left(\frac{f_l}{f_{co}}\right)^{b_1} \quad (23)$$

639
$$\frac{\varepsilon'_{cu}}{\varepsilon_{co}} = c_2 + k_4 \left(\frac{f_l}{f_{co}}\right)^{b_2} \quad (24)$$

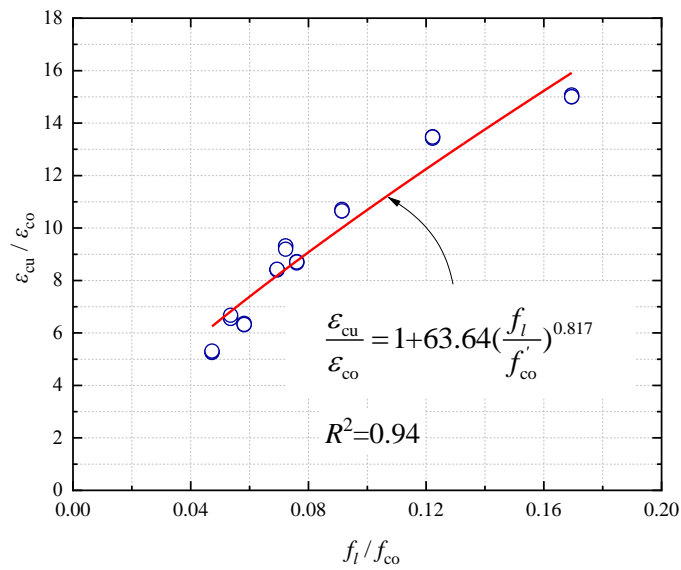
640 Where f'_{cu} and ε'_{cu} are the ultimate stress and the corresponding ultimate strain of PFRP-
 641 PVC-RAC-RCBA as UP point in Fig.15. Based on the regression analysis and iterative
 642 computations of the partial tested results, the fitting coefficients $c_1=1.17$, $b_1=-1.665$ and $k_3=-$
 643 0.0043 , $c_2=1$, $b_2=0.817$ and $k_4=63.64$ can be determined to create the strain equations for
 644 PFRP-PVC-RAC-RCBA, as illustrated in Fig.26. The strength and peak strain models can be
 645 expressed by Eq.(25) and (26):

646
 647
$$\frac{f'_{cu}}{f_{co}} = 1.17 - 0.0043 \left(\frac{f_l}{f_{co}}\right)^{-1.665} \quad (25)$$

648
$$\frac{\varepsilon'_{cu}}{\varepsilon_{co}} = 1 + 63.64 \left(\frac{f_l}{f_{co}}\right)^{0.817} \quad (26)$$

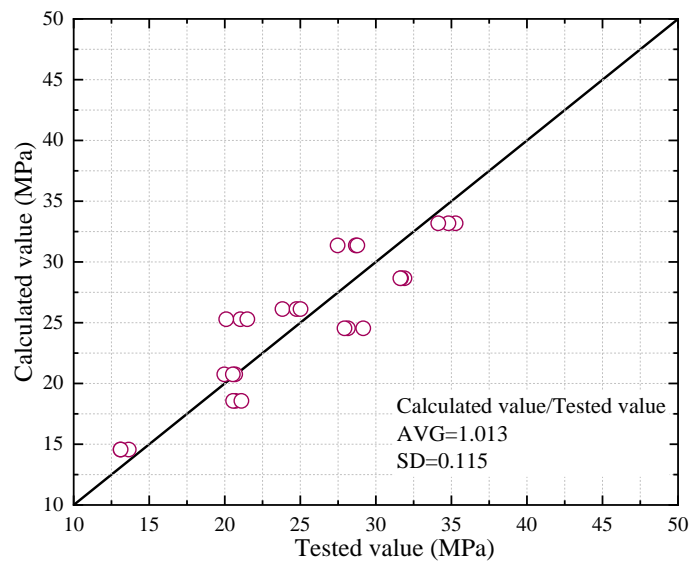


a) Fitting curves of ultimate stress model

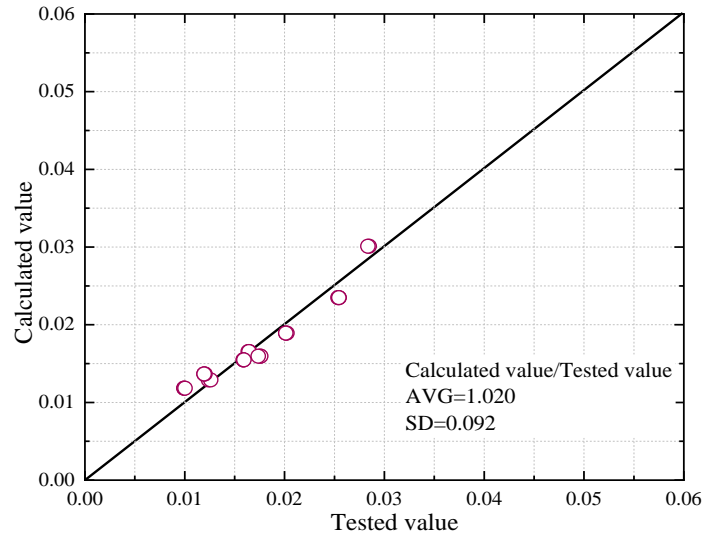


b) Fitting curves of ultimate strain model

Fig.26 Fitting curves of ultimate models



a) Fitting curves of ultimate stress model



b) Fitting curves of ultimate strain model
 Fig.27 Fitting curves of ultimate models

649

650 Based on the ultimate stress and strain equations above, the comparison in the ultimate stress
 651 and the ultimate axial strain between the experimental and predictions is shown in Fig 27. It
 652 can be seen that the predictions based on the developed stress and strain models matched the
 653 experimental stress and strain values of the PFRP-PVC-RAC-RCBA well, with relatively
 654 small deviations.

655

656 5 Conclusions

657 This paper investigated the axial compression behavior of polyester FRP-PVC tube encased
 658 recycled aggregate concrete (RAC) with recycled clay brick aggregates (RCBA). Two
 659 experimental phases were carried out. In the first stage, different replacement ratios of
 660 recycled aggregates and different cement-water ratios for RAC-RCBAs were considered in
 661 order to find out the optimized relationship between the strength of RAC and replacement
 662 ratios and cement-water ratios. In the second stage, experimental works were carried out to
 663 investigate the effects of type of PFRP confinement (i.e. tube and strip), PFRP thickness and
 664 spacing of PFRP strips on the axial compressive behavior of PFRP-PVC-RAC-RCBA
 665 specimens. The study reveals that:

666 1. The compressive strength of RAC-RCBA decreased with an increase of the water-cement
 667 ratios. The RAC-RCBA with 70% replacement ratio of RAs obtained the highest
 668 compressive strength. In general, the compressive strengths of all the RAC-RCBAs were
 669 lower than that of the NAC. The failure mode of RAC-RCBA was similar to that of NAC.
 670 However, the close-up showed that most of the RCBA coarse aggregates in the RAC
 671 were broken under compression but this was not observed for the natural coarse
 672 aggregates in the NAC. This is attributed to the much larger crushing of the RAs with
 673 RCBA than that of the NAs for NAC.

674 2. The PFRP tube, PFRP-strip-PVC tube and PFRP-tube-PVC tube confinement all
 675 increased the load carrying capacity and ductility of the RAC-RCBA remarkably. The
 676 PVC tube confinement did not show enhancement in the compressive strength but
 677 resulted in significant enhancement in the ductility. In general, the enhancement in
 678 compressive strength and ductility by PFRP-PVC tube dual confinement was larger than
 679 those of the corresponding PFRP or PVC tube single confinement, i.e. the increment in
 680 strength of RAC-RCBA by the 6-layer PFRP tube-PVC confinement was 34.2%, while
 681 that of RAC-RCBA by 6-layer PFRP or PVC tube alone was 26.0% and 0.1%,
 682 respectively.

683 3. The improvement on strength and ductility for the RAC-RCBA by the PFRP-PVC
 684 confinement was increase with an increasing PFRP tube thickness and a decreasing

685 spacing of the PFRP strip. In addition, the PFRP tube-PVC-RAC-RCBA always exhibited
686 higher compressive strength and ultimate strain than those of the corresponding PFRP
687 strip-PVC-RAC-RCBA with the same PFRP thickness. However, the PFRP strip-PVC-
688 RAC-RCBA showed the same compressive stress-strain curve pattern with the PFRP
689 tube-PVC-RAC-RCBA.

690 4. The comparison with the GFRP tube RAC-RCBA and CFRP tube RAC-RCBA showed
691 that GFRP and CFRP confinement resulted in much higher enhancement in the
692 compressive strength compared with PFRP, PVC and PFRP-PVC for RAC-RCBA due to
693 the much larger tensile strength and modulus of the GFRP and CFRP. However, the
694 PFRP and PFRP-PCV confinement resulted in much larger ductility compared with their
695 GFRP and CFRP confinement counterparts.

696 5. Design-oriented stress-strain models were developed for PFRP-PVC-RAC-RCBA
697 specimens in axial compression. The accuracy of the developed models was verified with
698 the experimental results.

699 Overall, this study confirmed that the PFRP-PVC-RAC-RCBA hybrid system is quite
700 promising for structural application with desirable carrying capability and ductility
701 characteristic. In the future study, the effects of different experimental parameters such as size
702 effect and slenderness ratio of the specimens on axial compression and even dynamic loading
703 responses need to be evaluated.
704

705 **Acknowledgement**

706 This study is supported by National Key Research and Development Program of China (No.
707 2017YFC0703305) and Federal Ministry of Education and Research of Germany (No.
708 01DS18023).

709

710 **References**

711 [1] Ghisellini P, Ji X, Liu GY, Ulgiati S. Evaluating the transition towards cleaner production
712 in the construction and demolition sector of China: A review. *Journal of Cleaner*
713 *Production* 2018;195: 418-434

714 [2] Nezerka V, Hrbek V, Prosek Z, Somr M. Micromechanical characterization and
715 modelling of cement pastes containing waste marble power. *Journal of Cleaner*
716 *Production* 2018;195: 1081-1090.

717 [3] J.L. Chen. Reconsideration of issues about construction waste recycling. *Construction*
718 *Technology*. 2015;58-59.

719 [4] J.L. Chen, W.J. Zhou, W. Li. Precondition and problems in reutilization of building
720 wastes. *Architecture Technology*. 2015;46(12):1114-1116.

721 [5] T.U. Mohammed, A. Hasnat, M.A Awal. Recycling of brick aggregate concrete as coarse
722 aggregate. *Journal of Materials in Civil Engineering*. 2014;27(7): B4014005.

723 [6] J. Yang, Q. Du, Y.W. Bao. Concrete with recycled concrete aggregate and crushed clay
724 bricks. *Construction and Building Materials*. 2011;25:1935-1945.

725 [7] C.S Poon., Z.H. Shui, L Lam. Effect of microstructure of ITZ on compressive strength of
726 concrete prepared with recycled aggregates. *Construction and Building Materials*. 2004;
727 18(6): 461-468.

728 [8] M. Etxeberria, E. Vázquez, A. Marí. Influence of amount of recycled coarse aggregates
729 and production process on properties of recycled aggregate concrete. *Cement and*
730 *concrete research*. 2007;37(5):735-742.

731 [9] Akhtat A, Sarmah A. Strength improvement of recycled aggregate concrete through
732 silicon rich char derived from organic waste. *Journal of Cleaner Production* 2018;196:
733 411-423.

734 [10] X. Sun, L. Yan, Kasal B. Impact behavior of concrete columns confined by both GFRP
735 tube and steel spiral reinforcement. *Construction and Building Materials*. 2017;131:438-
736 448.

- 737 [11] L. Yan, N. Chouw, K. Jayaraman. Effect of column parameters on flax FRP confined
738 coir fibre reinforced concrete. *Construction and Building Materials*. 2014;55:299-312.
- 739 [12] L. Yan, N. Chouw. Natural FRP tube confined fibre reinforced concrete under pure axial
740 compression: A comparison with glass/carbon FRP. *Thin-Walled Structures*.
741 2014;82:159-169.
- 742 [13] G. Ma, H. Li. Testing and analysis of basalt FRP-confined damaged concrete cylinders
743 under axial compression loading. *Construction and Building Materials*. 2018;169:762-
744 774.
- 745 [14] L. Yan, N. Chouw. Experimental study of flax FRP tube encased coir fibre reinforced
746 composite column. *Construction and Building Materials*. 2013;40:1118-1127.
- 747 [15] A. Duchez. Effect of bond on compressive behavior of flax fibre reinforced polymer
748 tube-confined coir fibre reinforced concrete. *Journal of Reinforced Plastics and*
749 *Composites*. 2013;32:273-285.
- 750 [16] L. Huang, P. Yin, L. Yan, B. Kasal. Behavior of hybrid GFRP-perforated-steel tube
751 encased concrete under uniaxial compression. *Composite Structures*. 2016;142:313-324.
- 752 [17] C. Gao, L. Huang, L. Yan, G. Ma, L. Xu, Compressive behavior of CFFT with inner
753 steel wire mesh, *Composite Structures*. 2015;133:322-330.
- 754 [18] L. Huang, X. Xun, D. Zhu. Compressive behavior of concrete confined with GFRP
755 tubes and steel spirals. *Polymers*. 2015;7 (5):851-875.
- 756 [19] L. Huang, D. Zhu. Compressive behavior of concrete confined by CFRP and transverse
757 spiral reinforcement. Part A: experimental study. *Material Structures*. 2016;49(3):1001-
758 1011.
- 759 [20] J. Xiao, Y. Huang, J. Yang. Mechanical properties of confined recycled aggregate
760 concrete under axial compression. *Construction and Building Materials*. 2012;26(1): 591-
761 603.
- 762 [21] C. Gao, L. Huang, L. Yan, B. Kasal, W. Li. Behavior of glass and carbon FRP tube
763 encased recycled aggregate concrete with recycled clay brick aggregate. *Composite*
764 *Structures*. 2016;155:245-254.
- 765 [22] T. Xie, T. Ozbakkaloglu. Behavior of recycled aggregate concrete-filled basalt and
766 carbon FRP tubes. *Construction and Building Materials*. 2016;105:132-143.
- 767 [23] G.M. Chen, Y.H. He, T. Jiang. Behavior of CFRP-confined recycled aggregate concrete
768 under axial compression. *Construction and Building Materials*. 2016;111:85-97.
- 769 [24] M.S.I. Choudhury, A.F.M.S. Amin, M.M. Islam, A. Hasnat. Effect of confining pressure
770 distribution on the dilation behavior in FRP-confined plain concrete columns using stone,
771 brick and recycled aggregates. *Construction and Building Materials*. 2016;102(1):541-
772 551.
- 773 [25] Ardavan Yazdanbakhsh, Lawrence C.B. The effect of shear strength on load capacity of
774 FRP strengthened beams with recycled concrete aggregate. *Construction and Building*
775 *Materials*. 2016;102(1):133-140.
- 776 [26] R.D. Freeman, J.L. Burati, S.N. Amirkhanian. Polyester fibers in asphalt paving
777 mixtures. *Association of Asphalt Paving Technologists Proc*. 1989;58.
- 778 [27] Z. Jing, Z. Bayasi. Properties of polyester fiber reinforced concrete. *Journal of Dalian*
779 *University of Technology*. 1993;S2.
- 780 [28] T. Ochi, S. Okubo, K. Fukui. Development of recycled PET fiber and its application as
781 concrete-reinforcing fiber. *Cement and Concrete Composites*. 2007;29(6):448-455.
- 782 [29] J.H.J. Kim, C.G. Park, S.W. Lee. Effects of the geometry of recycled PET fiber
783 reinforcement on shrinkage cracking of cement-based composites. *Composites Part B:*
784 *Engineering*. 2008;39(3): 442-450.
- 785 [30] De Oliveira L.A.P, Castro-Gomes J.P. Physical and mechanical behavior of recycled
786 PET fibre reinforced mortar. *Construction and Building Materials*. 2011;25(4):1712-1717.
- 787 [31] R.P. Borg, O. Baldacchino, L. Ferrara. Early age performance and mechanical
788 characteristics of recycled PET fibre reinforced concrete. *Construction and Building*
789 *Materials*. 2016;108:29-47.
- 790 [32] J.G. Dai, Y.L. Bai, J.G. Teng. Behavior and Modeling of Concrete Confined with FRP

- 791 Composites of Large Deformability. *Journal of Composites for Construction*. 2011;
792 15(6):963-973.
- 793 [33] Ispir M. Monotonic and cyclic compression tests on concrete confined with PET-FRP.
794 *Journal of Composites for Construction*. 2014;19(1): 04014034.
- 795 [34] S. Saleem, Q. Hussain, A. Pimanmas. Compressive behavior of PET FRP-confined
796 circular, square, and rectangular concrete columns. *Journal of Composites for*
797 *Construction*. 2016;21(3): 04016097.
- 798 [35] S. Saleem, A. Pimanmas, W. Rattanapitikon. Lateral response of PET FRP-confined
799 concrete. *Construction and Building Materials*. 2018;159: 390-407.
- 800 [36] A. Pimanmas, S. Saleem. Dilation Characteristics of PET FRP-Confined Concrete.
801 *Journal of Composites for Construction*. 2018;22(3): 04018006.
- 802 [37] L. Huang, X. Yang, L. Yan, K. He, H. Li, Y. Du. Experimental study of polyester fiber-
803 reinforced polymer confined concrete cylinders. *Textile Research Journal*. 2016;
804 86(15):1606-1615.
- 805 [38] L. Huang, L. Chen, L. Yan. Behavior of polyester FRP tube encased recycled aggregate
806 concrete with recycled clay brick aggregate: Size and slenderness ratio effects.
807 *Construction and Building Materials*. 2017;154:123-136.
- 808 [39] T.A. Ranney, L.V. Parker. Susceptibility of ABS, FEP, FRE, FRP, PTFE, and PVC well
809 casings to degradation by chemicals. Cold Regions Research and Engineering Lab
810 Hanover NH. 1995.
- 811 [40] Al Malaika S., Golovoy A., Wilkie C.A. Chemistry and technology of polymer additives.
812 Blackwell Science. 1999.
- 813 [41] Awham M.H., Salih Z.G.M. A study of some mechanical behavior on a thermoplastic
814 material. *Journal of Al-Nahrain University*. 2011;14(3):58-65.
- 815 [42] Rohe F.P.S. Strength testing of thermal welded PVC geomembrane field seams using
816 non-destructive air channel methods. Environmental Protection, Inc.
- 817 [43] Nowack R., Otto O.I., Braun E.W. 60 jahre erfahrungen mit rohrleitungen aus
818 weichmacherfreiem polyvinylchlorid (PVC-U). *KRV Nachrichten*. 1995;1-95.
- 819 [44] Ranney T.A., Parker L.V. Susceptibility of ABS, FEP, FRE, FRP, PTFE, and PVC Well
820 Casing to Degradation by Chemical. Special Report 95-1, US Army Corps of
821 Engineerings, January 1995.
- 822 [45] Kurt C. E. Concrete filled structural plastic columns. *Journal of the Structural Division*,
823 1978, 104 (ASCE 13478 Proceeding).
- 824 [46] H. Toutanji. Behavior of concrete columns encased in PVC-FRP composite tubes.
825 *Advanced Materials in Bridges and Structures (ACMBS-III)*. 2000;809-817.
- 826 [47] H. Toutanji, M. Saafi. Durability studies on concrete columns encased in PVC-FRP
827 composite tubes. *Composite Structures*. 2001;54(1): 27-35.
- 828 [48] Toutanji H., Saafi M. Stress-strain behavior of concrete columns confined with hybrid
829 composite materials. *Materials & Structures*, 2002, 35(6):338-347.
- 830 [49] Wang J., Yang Q. Experimental study on mechanical properties of concrete confined
831 with plastic pipe. *ACI Mater J*. 2010;107(2).
- 832 [50] Gupta P.K., Verma V.K. Study of concrete-filled unplasticized poly-vinyl chloride tubes
833 in marine environment. *Proc Inst Mech Eng Part M J Eng Marit Environ*.
834 2014;1475090214560448.
- 835 [51] Gathimba Naftary K., Oyawa Walter O., Mang'uriu Geoffrey N. Compressive strength
836 characteristics of concrete-filled plastic tubes short columns. *Int J Sci Res (IJSR)*.
837 2014;3(9):2168-2174.
- 838 [52] Jiang S.F., Ma S.L., Wu Z.Q. Experimental study and theoretical analysis on slender
839 concrete-filled CFRP-PVC tubular columns. *Construction and Building Materials*.
840 2014;53:475-487.
- 841 [53] GB/T 25177-2010. Recycled coarse aggregate for concrete. Standardization
842 Administration of The People's Republic of China. 2011.
- 843 [54] D. ASTM. Standard test method for tensile properties of polymer matrix composite
844 materials. 2008.

- 845 [55] GB/T 8804.2-2003. Thermoplastic pipes-Determination of tensile properties-Part 2:
846 Pipes made of unplasticized poly (vinyl chloride) (PVC-U), chlorinated poly (vinyl
847 chloride) (PVC-C) and high-impact poly (vinyl chloride) (PVC-HI). General
848 Administration of Quality Supervision, Inspection and Quarantine of the People's
849 Republic of China. 2003.
- 850 [56] Zhao L.J., Weng J.L., Chen W. Test and research on the double horizontal shaft
851 vibrating mixing technology. *Construction Machinery Technology and Management*.
852 2013;2:107-110.
- 853 [57] Feng X.N., Feng Z.X., Wang W.Z. Review on concrete vibratory mixing techniques.
854 *Chinese Journal of Construction Machinery*. 2007;5(1):113-116.
- 855 [58] T. Ozbakkaloglu. Compressive behavior of concrete-filled FRP tube columns:
856 Assessment of critical column parameters. *Engineering Structures*. 2013;51:188-199.
- 857 [59] M. Fakharifar, G. Chen. Compressive behavior of FRP-confined-filled PVC tubular
858 columns. *Composite Structures*. 2016;141:91-109.
- 859 [60] J.G. Teng, Y. Tao, W.Y. Long, S.L. Dong, Y.F. Yang. Behavior of hybrid FRP-
860 concrete-steel tubular columns: experimental and theoretical studies. *Progress in steel*
861 *building structures*. 2006;8(5):1-7.
- 862 [61] Pantelides C.P., Yan Z. Confinement model of concrete with externally bonded FRP
863 jackets or post tensioned FRP shells. *Journal of Structural Engineering*.
864 2007;133(9):1288-1296.
- 865 [62] Xiao Y., Wu H. Compressive behavior of concrete confined by various types of FRP
866 composite jackets. *Journal of Reinforced Plastics and Composites*. 2003;22(13):1187-
867 1201.
- 868 [63] L. Huang, C. Gao, L.B. Yan, B. Kasal, G. Ma. Reliability assessment of confinement
869 models of carbon fiber reinforced polymer-confined concrete. *Journal of Reinforced*
870 *Plastics and Composites*. 2016;0(0):1-31.
- 871 [64] L. Huang, C. Gao, L.B. Yan, B. Kasal, G. Ma, H.Z. Tan. Confinement models of GFPR-
872 confined concrete: Statistical analysis and unified stress-strain models. *Journal of*
873 *Reinforced Plastics and Composites*. 2016;0(0):1-25.
- 874 [65] P.P. Li. The research of mechanical behavior of BFRP-PVC tube self-compacting
875 recycled concrete short column under uniaxial compression. Liaoning University of
876 Technology. 2015.
- 877 [66] Spoelstra M.R., Monti G. FRP-confined concrete model. *Journal of Structural*
878 *Engineering*. 1999;9(4):143-150.
- 879 [67] Jian C. Lim, T. Ozbakkaloglu. Lateral strain to axial strain relationship of confined
880 concrete. *Engineering Structures*. 2015;141(5):04014141.
- 881 [68] Riccio A., Di Costanzo C., Di Gennaro P., Sellitto A., Raimondo A. Intra-laminar
882 progressive failure analysis of composite laminates with a large notch damage.
883 *Engineering Failure Analysis*. 2017;73:97-112.
- 884 [69] Riccio A., Sellitto A., Saputo S., Russo A., Zarrelli M., Lopresto V. Modelling the
885 damage evolution in notched omega stiffened composite panels under compression.
886 *Composites Part B-Engineering*. 2017;126:60-71.
- 887 [70] Riccio A., Damiano M., Raimondo A., Di Felice G., Sellitto A. A fast numerical
888 procedure for the simulation of inter-laminar damage growth in stiffened composite
889 panels. *Composite Structures*. 2016;145:203-216.
- 890 [71] Campione G., La Mendola L., Monaco A., Valenza A., and Fiore V. Behavior in
891 compression of concrete cylinders externally wrapped with basalt fibers. *Composites:*
892 *Part B*. 2015;69:576-586.
- 893 [72] De Santis S., De Felice G., Napoli A., and Realfonzo R. Strengthening of structures with
894 Steel Reinforced Polymers: A state-of-the-art review. *Composites: Part B*. 2016;104:87-
895 110.
- 896